Liquid Crystals
Publication details, including instructions for authors and subscription information:
http://www.informaworld.com/smpp/title~content=t713926090

Microstructure and dynamics in lyotropic liquid crystals. Principles and applications of nuclear spin relaxation

Bertil Halle[a]; Per-Ola Quist[a]; István Furó[a]
[a] Condensed Matter Magnetic Resonance Group, Physical Chemistry 2, Lund University, Lund, Sweden

To cite this Article Halle, Bertil , Quist, Per-Ola and Furó, István(1993) 'Microstructure and dynamics in lyotropic liquid crystals. Principles and applications of nuclear spin relaxation', Liquid Crystals, 14: 1, 227 — 263
To link to this Article: DOI: 10.1080/02678299308027314
URL: http://dx.doi.org/10.1080/02678299308027314

LIQUID CRYSTALS, 1993, VOL. 14, NO. 1, 227–263

Invited Lecture

Microstructure and dynamics in lyotropic liquid crystals
Principles and applications of nuclear spin relaxation

by BERTIL HALLE*, PER-OLA QUIST and ISTVÁN FURÓ
Condensed Matter Magnetic Resonance Group,
Physical Chemistry 2, Lund University,
P.O. Box 124, S-22100 Lund, Sweden

Nuclear spin relaxation of quadrupolar nuclei provides access to a wide range of properties of lyotropic liquid crystals, ranging from the molecular ordering and dynamics at the interface to the macroscopic viscoelastic behaviour. We emphasize here the unique capability of the spin relaxation method to provide detailed geometric and dynamic information relating to the microstructure of lyotropic liquid crystals, i.e. the metric, curvature, and fluctuations of the dividing interface that separates polar and non-polar regions. This information is conveyed to the spin system via the translational diffusion of surfactants or counterions over the interface. The general principles of the spin relaxation method, as applied to lyotropic liquid crystals, are described, with emphasis on the model-independent information content of the relaxation observables and on the relation to microstructure. Specific results for lamellar, hexagonal, cubic, and nematic phases are also described.

1. Introduction

Lyotropic liquid crystals present a wider repertoire of phase behaviour than any other state of matter [1–10]. The catalogue of lyotropic mesophases is steadily growing, now comprising more than a dozen crystallographically distinct phases. For example, the binary systems sodium dodecyl sulphate/water [11] and potassium palmitate/water [12] each features six distinct mesophases. Ternary lyotropic systems exhibit an even greater phase variety; for example, there are three distinct nematic phases in the system potassium laurate/water/decanol [13] and five distinct cubic phases in the system didodecyldimethyl ammonium bromide/water/styrene [14].

The rich phase polymorphism of lyotropic liquid crystals is related to the fact that they are association colloids; surfactant self-assembly leads to a hierarchy of structural organization. At the highest level are the rotational and translational symmetries that determine the crystallographic space group of the mesophase. At the intermediate level is the microstructure, which may be defined as the topology and local geometry (dimensions and curvatures) of the dividing interface that separates polar and non-polar regions. The microstructure can be radically different in phases belonging to the same space group. In fact, the microstructure can even vary (qualitatively) within a given phase, in response to changes in temperature and composition [15–24]. Such variations may be generally viewed as intrinsic (thermodynamically stable) structural defects, as opposed to metastable (for example, domain boundaries) and surface induced (for example, focal conics) [25] defects. The microstructure may also be taken

*Author for correspondence

0267-8292/93 $10·00

to include thermal fluctuations on supramolecular length scales, for example, smectic bilayer undulations and orientational disorder of nematic aggregates.

At the lowest level of the structural hierarchy is the molecular ordering of the various components with respect to the local interface, for example, the orientational order of surfactant chains and interfacial water, and the spatial inhomogeneity in the counterion distribution. These local properties of lyotropic liquid crystals are by now reasonably well understood. In the following we focus instead on the microstructure, which is far less completely understood.

Among the numerous experimental techniques that have contributed to the understanding of lyotropic liquid crystals, scattering experiments (thermal neutrons, X-rays, and visible light) and nuclear magnetic resonance (NMR) are probably the most powerful and versatile ones. Both techniques can furnish information about each of the three levels of structural organization, but in a complementary way; they are often profitably used in conjunction.

The NMR experiments that have been used to study lyotropic liquid crystals can be broadly classified into three categories. Lineshape studies are now used routinely to distinguish between cubic, uniaxial, and biaxial mesophases and between calamitic and discotic nematic phases and to monitor the nature and degree of phase alignment in macroscopically oriented samples. In non-cubic phases, the lineshape, in particular the static splitting, contains information about all three levels of organization. In general it is not possible to separate this information, but if the microstructure is known, the local molecular ordering can be characterized [7, 26–29]. Conversely, if the local contribution can be estimated (for example, from measurements on another mesophase), information about the microstructure can be derived from the diffusional averaging of the lineshape. This approach is particularly informative for biaxial phases [30–33], since the powder lineshape then involves two independent microstructure-related parameters. In polymerized lyotropic mesophases, where surface diffusion of surfactant molecules is prevented, the lineshape provides an even more detailed picture of the microstructure [34].

The second type of NMR experiment is the (pulsed) field gradient spin echo experiment, used for diffusion studies [35–37]. Such measurements can yield the principal components of the macroscopic diffusion tensor for the various molecular species in the mesophase [38–41]. Since this experiment measures displacements over macroscopic distances (typically, several μm) it can provide information about the microstructure, which imposes constraints on the diffusion paths. In particular, diffusion studies can often be used to establish the topology of the microstructure, i.e. whether the polar or apolar regions are closed or macroscopically continuous in one, two, or three dimensions.

The third type of NMR experiment is the nuclear spin relaxation experiment, which is our main concern here. Among the three types of NMR experiment, this is potentially the most informative, but the most demanding. The spin relaxation behaviour reflects structure as well as dynamics at all three levels of the hierarchy. Since the pioneering work of Charvolin and Rigny 20 years ago [42], most spin relaxation studies of lyotropic liquid crystals have focused on ordering and dynamics at the molecular level in phases of known microstructure [43–51]. Most relaxation studies of phospholipid bilayers [52–61] also belong to this category. Our present concern, however, is with spin relaxation studies that focus on microstructure and surface diffusion in lyotropic liquid crystals. About a dozen such studies, of cubic [62–67], hexagonal [68–70], lamellar [71], and nematic [72, 73] mesophases, have so far been reported.

Much of the experimental sophistication required for spin relaxation studies of lyotropic liquid crystals utilizing spin $I = 1$ nuclei, such as ^2H and ^{14}N, was developed in connection with studies of polymers [74], thermotropic liquid crystals [75, 76], and biological membranes [53, 55]. Nuclei of higher spin, mainly counterion nuclei with $I = 3/2$, 5/2, and 7/2, are also of interest, and spin relaxation experiments appropriate for such high spin nuclei have recently been devised [77–81]. In § 2 we discuss the nature of the spin relaxation observables and some of the methods used to measure them.

As discussed in § 3, the spin relaxation depends on the orientation of the (macroscopically aligned) liquid crystal with respect to the static magnetic field and it is only by studying this relaxation anisotropy that the full information content accessible by spin relaxation can be disclosed. The amount of available information is dictated by the point group symmetry of the liquid crystal. In a uniaxial mesophase, for example, nine distinct model-independent quantities can be determined from spin relaxation experiments at a single magnetic field. Field variation, of course, yields additional information.

In §§ 4 and 5 we describe how spin relaxation experiments provide information about microstructure in lyotropic liquid crystals. The basic idea is to study nuclei residing in surfactant molecules or counterions that are effectively confined to the interface. Quadrupolar spin relaxation is due to fluctuations of the orientation and magnitude of the electric field gradient tensor at the nuclear site [82]. The local motions project this tensor on to the local interface normal and as the spin-bearing species diffuses over the curved interface the orientation of the residual (projected) field gradient fluctuates, thereby inducing spin relaxation. Since the amplitude and rate of these fluctuations depend on the geometry of the interface, surface diffusion reflects the microstructure of the mesophase. Fluctuations of the microstructure itself, such as nematic director fluctuations, also contribute to the spin relaxation (see § 6) as do various kinds of local motion. Fortunately, the time scales of these processes are sufficiently different that their contributions to the spin relaxation can be separated.

Finally, in § 7, we illustrate the general principles outlined in §§ 2–6 by specific case studies taken from each of the four basic types of lyotropic liquid crystal: nematic mesophases and translationally ordered mesophases periodic in one, two, and three dimensions.

2. Relaxation observables

2.1. *Nuclear quadrupole coupling in anisotropic fluids*

Most lyotropic liquid crystals present the NMR spectroscopist with a choice of nuclear isotopes suitable for spin relaxation experiments. To be a sensitive probe of microstructure, the nucleus should be effectively confined to the interface. In practice this restricts the choice to (i) surfactant headgroup nuclei (for example, ^{14}N), (ii) counterion nuclei (for example, ^{23}Na), and (iii) ^2H nuclei selectively introduced in the α-position (next to the headgroup) of the surfactant alkyl chain.

The nuclei of interest, such as ^2H, ^{14}N, and ^{23}Na (along with most other counterion nuclei) have either spin $I = 1$ or half-integral spin $I \geqslant 3/2$ and are coupled to the molecular degrees of freedon *via* the interaction of the nuclear electric quadrupole moment with the electric field gradient generated by the surrounding charge distribution [82]. This quadrupole coupling conveys to the spin system a wealth of structural and dynamic information.

The first order effect of the quadrupole coupling is to shift the Zeeman energy levels, thereby splitting the resonance line of a spin-I nucleus into $2I$ equidistant lines. This quadrupole splitting, which occurs in mesophases of lower than cubic symmetry, contains information about the microstructure in the phase. In all but the simplest cases, however, the quadrupole splitting yields a non-separable product of quantities related to the different levels of the structural hierarchy. The ^{2}H quadrupole splitting from an α-deuteriated surfactant in a uniaxial nematic phase, for example, is a product of (i) a parameter describing the local order of the C–D bond with respect to the aggregate surface, (ii) a geometrical factor reflecting the aggregate shape, and (iii) a parameter describing the orientational ordering of the surfactant aggregates comprising the nematic fluid [27]. These factors cannot be separated without recourse to additional data, for example, spin relaxation rates [72].

The principal second order effect of the quadrupole coupling is to induce spin relaxation, characterized by spin relaxation rates. Most familiar are the longitudinal and transverse relaxation rates R_1 and R_2 associated with the magnetization vector components parallel and perpendicular, respectively, to the static magnetic field. While R_1 and R_2 suffice to describe the relaxation behaviour of $I=1$ nuclei in isotropic fluids, more rate constants are in general needed for $I>1$ nuclei and (even for $I=1$ nuclei) in anisotropic fluids such as liquid crystals. This complication, which greatly enhances the potential of the spin relaxation technique, arises because a system of spin-I nuclei admits non-equilibrium states with magnetic tensor polarization [83, 84] of rank $k=1, 2, \ldots, 2I$, where $k=1$ is the usual vector (dipole) magnetization. In non-cubic liquid crystals (with a non-zero quadrupole splitting) spin states of any rank up to $2I$ can be produced, whereas in cubic liquid crystals and isotropic fluids only states of odd tensor rank can exist. The various spin states can be formally described in terms of spherical multipoles of rank k and projection index $q=0, \pm 1, \ldots, \pm k$. The axial ($q=0$) multipole components, referred to as polarizations or alignments, are the generalizations of the longitudinal magnetization ($k=1$, $q=0$). The remaining ($q\neq 0$) multipole components, referred to as q-quantum coherences, are the generalizations of the transverse magnetization ($k=1$, $q=\pm 1$).

2.2. *Time correlation functions and spectral densities*

All the information about liquid crystal microstructure and dynamics that can be derived from the spin relaxation rates is contained in time correlation functions (TCFs) of the form

$$G^L_{kk'}(\tau)=\langle V^{L*}_k(0)V^L_{k'}(\tau)\rangle-\langle V^{L*}_k\rangle\langle V^L_{k'}\rangle, \tag{2.1}$$

where $V^L_k(\tau)$ is the kth spherical component with respect to a lab-fixed frame (where the static magnetic field defines the z axis) of the electric field gradient (EFG) tensor. We assume that the standard second order spin relaxation theory is valid [82], and that the quadrupole coupling is the only source of spin relaxation.

The (stochastic) time dependence of the EFG components reflects thermal motions in the liquid crystal. Since the EFG tensor is of rank two, there are 25 TCFs of the form of equation (2.1) ($k,k'=0, \pm 1, \pm 2$). Time reversal invariance reduces this number to 15. Considerations of rotational symmetry lead to further simplification. In an isotropic fluid, there is only one distinct TCF, whereas in a uniaxial liquid crystal aligned with the static magnetic field there are three: the diagonal TCFs $G^L_{kk}(\tau)$ with $k=0, 1, 2$. For a liquid crystal of arbitrary symmetry and orientation, the off-diagonal TCFs do not vanish by symmetry. However, as long as the spin relaxation rates and the residual

quadrupole coupling are small compared to the Larmor frequency, which is the case except in extremely weak magnetic fields, the off-diagonal TCFs can be neglected ('secular approximation'), so that only the three diagonal TCFs $G^L_{kk}(\tau)$ remain [85].

Under the rather mild conditions stipulated above, the entire spin relaxation behaviour is governed by the three lab-frame spectral densities (LFSDs)

$$J^L_{kk}(k\omega_0) = \int_0^\infty d\tau \cos(k\omega_0\tau)\, G^L_{kk}(\tau). \tag{2.2}$$

The adiabatic (zero frequency) spectral density $J^L_{00}(0)$ contains contributions from motions on all time scales (within the motional narrowing regime [82]), while the non-adiabatic spectral densities $J^L_{11}(\omega_0)$ and $J^L_{22}(2\omega_0)$ are affected only by motions on the time scale of the inverse Larmor frequency $1/\omega_0$ or faster.

2.3. *Spin relaxation rates*

The theoretical description of a spin relaxation experiment accounting for the spin dynamics during radio-frequency (RF) pulses and during periods of free evolution, is particularly simple if (i) the RF pulses are non-selective (hard), which usually implies that the quadrupole splitting is small compared to the Larmor frequency, and (ii) the quadrupole splitting is large compared to the non-adiabatic linewidths (cf. below). (For cubic mesophases, less restrictive conditions apply.) Under these conditions, which are usually satisfied in studies of lyotropic liquid crystals, the RF pulses simply rotate the state multipoles, i.e. they mix the quantum order q without affecting the tensor rank k, whereas free evolution (under the quadrupole hamiltonian) mixes the rank without affecting the quantum order [83, 84]. In non-cubic liquid crystals the evolution of the polarizations ($q=0$) thus involves $2I$ generalized longitudinal relaxation rates. Among these $2I$ rates, $I+1/2$ describe the (coupled) evolution of the odd-rank polarizations and $I-1/2$ describe the (coupled) evolution of the even-rank polarizations [78]. This applies to half-integral I; for $I=1$ there is one odd-rank (Zeeman) and one even-rank (quadrupolar) longitudinal relaxation rate [55, 74–76]. The evolution of the coherences involve $I(2I+1)$ generalized transverse rates, all of which are not necessarily distinct. Under the condition (ii), the homogeneous linewidths in the q-quantum spectra are determined by 2, 2, 6, and 10 distinct transverse rates for $I=1, 3/2, 5/2$, and $7/2$, respectively [55, 75, 76, 80, 86].

The homogeneous linewidths (or transverse relaxation rates) of satellite peaks, i.e. spectral lines that exhibit a first order quadrupolar frequency shift, are adiabatic and can be expressed as linear combinations of the three LFSDs. The homogeneous linewidths of central peaks, i.e. spectral lines that are not quadrupole shifted to first order, are linear combinations of the two non-adiabatic LFSDs. The longitudinal relaxation rates are also non-adiabatic, but depend non-linearly on the LFSDs except in the special cases $I=1$ and $I=3/2$.

The number of distinct spin relaxation rates that can be determined from longitudinal relaxation experiments and homogeneous linewidths are summarized in table 1. (The explicit linear combinations of LFSDs can be found in [55, 74–76, 87] for $I=1$ and in [77–80, 86] for half-integral I.) Some additional relaxation observables of lesser importance are mentioned in §2.4. A complete set of relaxation observables, required to determine the three LFSDs, usually consists of three linearly independent relaxation rates chosen from table 1. The LFSDs may evidently be over-determined; either by measuring more than three linearly independent relaxation rates or by measuring the same linear combination in different types of relaxation experiment.

Table 1. The number of distinct spin relaxation rates for quadrupolar nuclei in anisotropic fluids.

Relaxation rate	$I=1$	$I=3/2$	$I=5/2$	$I=7/2$
Longitudinal	2	3	5	7
Transverse†	2	2	6	10
Adiabatic	1	1	3	6
Non-adiabatic	1	1	3	4

†From homogeneous linewidths only.

Such redundancy can be used to check systematic errors caused by instrumental limitations, mesophase alignment imperfections, or contributions from secondary (non-quadrupolar) relaxation mechanisms, or can be used simply to improve the accuracy in the determination of the three LFSDs.

2.4. *Spin relaxation experiments*

The basic objective of a complete spin relaxation study of a lyotropic liquid crystal is to determine the three LFSDs $J^L_{kk}(k\omega_0)$ with maximum accuracy and precision for a given measurement time. We consider here only macroscopically aligned (cf. § 3) non-cubic mesophases. (Cubic phases can be studied by the methods used for isotropic fluids.) Powder samples of non-cubic mesophases are unsuitable for relaxation studies due to the complete scrambling of the relaxation anisotropy in the smeared-out (poor signal to noise), overlapping satellites [77]. Although the full relaxation anisotropy information is present in a powder spectrum, deconvolution is probably not feasible in general.

The optimal choice of relaxation experiments for determining a complete set of relaxation observables depends on several factors, for example, the degree of mesophase alignment, the magnitudes of the quadrupole splitting and the LFSDs, the inhomogeneous broadening of the spectral lines, and the inhomogeneity in the RF field. A universal recipe therefore cannot be given. In most cases, however, the optimal choice will include longitudinal relaxation experiments as well as echo experiments for measuring homogeneous linewidths.

The classical longitudinal relaxation experiments are the inversion recovery (IR) and the Jeener–Broekaert (JB) experiments, which monitor the (coupled) evolution of odd-rank and even-rank polarizations, respectively [55, 74–76, 78]. The IR experiment is most useful for $I=1$ and $I=3/2$ nuclei, for which the recovery function can be calculated analytically. For $I=1$ the single-exponential recovery yields j_1+4j_2. (In this section we use the short-hand notation $j_k=J^L_{kk}(k\omega_0)$.) For $I=3/2$ the central line and satellites recover bi-exponentially in general, with the relative weights of the exponentials determined by the detection pulse(s). For a $\pi/2$ detection pulse angle, the satellites recover exponentially with a rate constant proportional to j_2. For $I=1$ and $I=3/2$ nuclei, the single exponential decay of the quadrupole polarization in the JB experiment yields j_1 and j_1+j_2, respectively. For $I=5/2$, a modified JB experiment has been devised that yields a difference-double-exponential satellite decay (due to the coupled evolution of the quadrupole and hexadecapole polarizations) with rate constants depending non-linearly on j_1 and j_2.

Measurements of the homogeneous linewidths associated with the various q-quantum Zeeman transitions usually require echo (refocusing) experiments to

eliminate static line broadening due to spatial inhomogeneities in the (static) quadrupole coupling (usually due to imperfect mesophase alignment) and in the magnetic field. A variety of echo experiments has been devised for measuring homogeneous single-quantum and multiple-quantum linewidths [68, 76, 77, 79–81, 88, 89]. While for $I = 1$ nuclei either 1D or 2D experiments can be performed, for $I \geqslant 3/2$ nuclei 2D experiments are indispensable. The non-adiabatic central linewidths (associated with the $-q/2 \leftrightarrow q/2$ transitions) are obtained from 2D spin echo (SE) experiments, while the adiabatic satellite linewidths are obtained from 2D quadrupolar echo (QE) experiments. (For α-deuteriated surfactants, the static ^2H–^1H dipole coupling to the strongly coupled proton spins further down the chain and the ^2H–^2H dipole coupling within the CD_2 group may give rise to complications [90].) By using appropriate phase cycles to filter out unwanted coherence pathways, 2D echo experiments can also be performed with semi-selective (or selective [91, 92]) RF pulses, allowing systems with large ($\geqslant 100$ kHz) quadrupole splittings to be studied [80, 81].

Some general guidelines for the choice of spin relaxation experiments can be given. For $I = 1$ nuclei the three LFSDs can be determined by performing the IR ($j_1 + 4j_2$), JB (j_1), and 2D QE experiments ($3j_0 + 3j_1 + 2j_2$), while the 2D SE experiment ($j_1 + 2j_2$) on the double-quantum coherence can provide useful redundancy. For $I = 3/2$ nuclei, with (essentially) non-selective RF pulses available, the single-quantum 2D SE ($j_1 + j_2$) and 2D QE ($j_0 + j_1 + j_2$) experiments can be combined with IR (j_2) and JB ($j_1 + j_2$) experiments on the satellites. If the satellites are too broad to give acceptable signal to noise, the intense central line can be utilized instead in IR experiments (j_1 and j_2) with short detection pulses and in a double-quantum 2D QE experiment ($j_0 + j_1 + j_2$). For $I > 3/2$ nuclei the homogeneous single-quantum linewidths, obtained from 2D echo experiments, are in principle sufficient to determine the three LFSDs. In practice, however, some multiple-quantum linewidths are also needed to obtain good accuracy. Multiple-quantum linewidths are also useful in general to assess contributions from possible secondary relaxation mechanisms. Finally, we note that Monte Carlo simulations can be useful for optimizing the choice of relaxation experiments and the fitting procedures used to analyse the raw data.

While the experiments discussed above are the most widely applicable ones for lyotropic liquid crystals, other, more specialized, relaxation experiments can sometimes be useful. Among these are the multiple echo experiments, so far used only with $I = 1$ nuclei [76, 93–97]. Such experiments can be used either to identify slow motions or to suppress their contribution to the adiabatic linewidths. Furthermore, in the case of a small quadrupole splitting, new relaxation pathways (connected with the off-diagonal elements in the coherence blocks of the relaxation matrix in the Zeeman basis) can be explored, giving access to new linear combinations of the three LFSDs. Relaxation experiments such as these, that use long RF pulse trains, are susceptible to cumulative errors due to pulse imperfections.

Another type of relaxation experiment that may be useful for studying lyotropic liquid crystals in the field cycling technique [98, 99], which allows determination of the non-adiabatic LFSDs over a wide range of frequencies, extending far below the MHz range normally accessible with conventional NMR spectrometers. Unfortunately, this technique is not easily applicable to the rapidly relaxing quadrupolar nuclei of interest in lyotropic liquid crystals. Field cycling studies of liquid crystals have therefore been essentially confined to proton relaxation [48, 60] (see, however, [100]).

A less well-known relaxation observable is the second order dynamic quadrupolar shift associated with the various q-quantum transitions [86, 101–103]. The dynamic

shifts, related to the sine transform of the TCF in equation (2.1), provide new information but are usually smaller than the linewidths and hence difficult to measure accurately.

3. Relaxation anisotropy and mesophase symmetry

For a system as complex as a lyotropic liquid crystal, the LFSDs $J^L_{kk}(k\omega_0)$ obtained from the spin relaxation experiments are usually not amenable to direct physical interpretation. Information about the microstructure and dynamics of the mesophase can then be obtained only at the cost of invoking model assumptions. For isotropic fluids, this is the only open road, but it is a treacherous one as attested by the literature on spin relaxation in complex fluids. For oriented liquid crystals, there is a safer road that avoids much of the model dependence in the interpretation: to measure the relaxation anisotropy, i.e. the dependence of the spin relaxation rates and LFSDs on the orientation of the liquid crystal with respect to the static magnetic field.

3.1. *Macroscopic orientation of lyotropic liquid crystals*

In NMR studies of liquid crystals the static magnetic field plays a dual role by interacting with the spin system as well as with the molecular system. The Zeeman interaction with the nuclear magnetic moments polarizes the spin system, while the interaction with the molecular anisotropic diamagnetic susceptibility tensor produces a macroscopic torque on the mesophase. For a uniaxial phase, the magnetic torque **T** is given by

$$\mathbf{T} = \mathbf{t}\frac{B_0^2}{2\mu_0}(\chi_\parallel^C - \chi_\perp^C)\sin(2\theta_{LC}), \tag{3.1}$$

where **t** is a unit vector orthogonal to the magnetic field $\mathbf{B}_0$ and to the mesophase director **n**. $\chi_\parallel^C$ and $\chi_\perp^C$ are the longitudinal and transverse principal components of the diamagnetic susceptibility tensor and θ_{LC} is the angle between B_0 and **n**. It follows from equation (3.1) that for mesophases with positive susceptibility anisotropy ($\chi_\parallel^C > \chi_\perp^C$) the magnetic torque tends to align the uniaxial phase with the field. If the susceptibility anisotropy is negative ($\chi_\parallel^C < \chi_\perp^C$) the torque tends to orient the phase perpendicular to the field.

For a lyotropic nematic phase in the B_0 field of a conventional NMR spectrometer the magnetic torque establishes a virtually complete macroscopic orientation on a time scale of minutes [9]. For most non-nematic lyotropic mesophases, however, the high viscosity makes magnetic mesophase orientation impractically slow. On the other hand, this means that if such a mesophase can somehow be oriented, its original orientation will be effectively frozen in on the time scale of a spin relaxation experiment, thus allowing studies of relaxation anisotropy. To study the relaxation in a nematic mesophase at other orientations than that dictated by the instantaneous magnetic field direction, more elaborate procedures must be adopted, for example, fast [104, 105] or slow [106–107] sample rotation or alignment by an alternating electric field [108] (which interacts with the anisotropic electric polarizability and/or conductivity [109] of the lytropic mesophase) or by magnetic and AC electric fields [109, 110].

Several techniques are available for producing quasi-permanent macroscopic orientation of highly viscous (non-nematic) mesophases. The simplest alternative, when the phase behaviour permits, is to magnetically align the sample at a temperature where it is sufficiently fluid, for example, in a nematic phase [69, 111–114] or in a two-phase region with small micro-crystallites in equilibrium with an isotropic solution phase [68, 115, 116]. As the sample is slowly brought into the desired (viscous)

mesophase by changing the temperature, it usually retains its macroscopic orientation. Another possibility might be to reduce the effective mesophase viscosity by ultrasonication.

Smectic mesophases can also be aligned between closely spaced parallel glass plates [117]. This technique does not normally produce a homeotropic orientation of hexagonal mesophases, which tend to acquire a 2D isotropic orientational distribution in the plane of the glass surface [111, 116]. The major drawbacks of the glass plate method are the signal to noise reduction (the sample consists mainly of glass) and the contamination risk. (The dry deposition technique commonly used with phospholipids [54, 118] is unsuitable for lyotropic mesophases, whose composition must be accurately known.) These problems can be somewhat alleviated by increasing the plate spacing (to *c.* 0·2 mm). In this way good homeotropic alignment has been achieved with a dilute lamellar phase cooled from an isotropic microemulsion phase [119], and with a lamellar phase cooled from a magneto-aligned nematic N_D^- phase [71].

3.2. *Crystal-frame spectral densities*

The intrinsic properties, such as microstructure and dynamics, of a macroscopically oriented liquid crystal do not depend significantly on its orientation with respect to the magnetic field. It must therefore be possible to reduce the LFSDs $J^L_{kk}(k\omega_0)$, which depend on this orientation, to more fundamental quantities that only depend on the intrinsic properties of the mesophase. This reduction is accomplished by transforming the EFG components in equation (2.1) from the lab frame (L) to the crystal frame (C),

$$V^L_k(\tau) = \sum_{n=-2}^{2} D^{2*}_{kn}(\Omega_{LC})\, V^C_n(\tau), \tag{3.2}$$

where $D^2_{kn}(\Omega_{LC})$ is an element of the second-rank Wigner rotation matrix and $\Omega_{LC} = (-, \theta_{LC}, \phi_C)$ are the Euler angles specifying the coordinate frame rotation [120]. (The first Euler angle is irrelevant within the secular approximation, where LFDS with $k \neq k'$ vanish.)

Combination of equations (2.1), (2.2), and (2.3) yields

$$J^L_{kk}(k\omega_0; \theta_{LC}, \phi_C) = \sum_n \sum_p d^2_{kn}(\theta_{LC}) d^2_{kp}(\theta_{LC}) \exp[i(p-n)\phi_C] J^C_{np}(k\omega_0). \tag{3.3}$$

The crystal-frame spectral densities (CFSDs) $J^C_{np}(k\omega_0)$, defined by equations (2.1) and (2.2) with obvious modifications, depend only on the intrinsic properties of the mesophase. (A qualification of this statement is made in §6.3.)

3.3. *Mesophase symmetry and irreducible spectral densities*

According to equation (3.3), each of the three LFSDs can be expressed as a linear combination of 15 CFSDs (when time reversal symmetry has been exploited). Depending on the point group symmetry of the mesophase, some of these 15 CFSDs may vanish while others may be linearly dependent. Group theoretical methods can be used to establish the number of independent CFSDs and their form [121–124]. The approach is analogous to that used in molecular quantum chemistry: we construct symmetry-adapted functions that transform as components of irreducible representations of the point group. The EFG components V_k in equation (2.1) are *spherical* tensor components; like the second-rank spherical harmonics they transform as the five components of the irreducible representation D^2 of the full rotation group. The tensor components V_k are thus adapted to the symmetry of isotropic fluids. For liquid crystals,

however, the CFSDs should be constructed from EFG tensor components adapted to the symmetry of the mesophase. Accordingly, we replace equation (3.3) by

$$J^L_{kk}(k\omega_0; \theta_{LC}, \phi_C) = \sum_{\lambda} F_{k\lambda}(\theta_{LC}, \phi_C)\, J^C_\lambda(k\omega_0), \tag{3.4}$$

where we have introduced a composite index $\lambda = (\alpha, \mu, \mu')$ for the irreducible representations α of the point group of the mesophase and the independent sub-spaces μ of α (if α occurs more than once in the decomposition of the reducible representation D^2).

The spectral densities $J^C_\lambda(k\omega_0)$ are the fundamental quantities in relaxation studies of anisotropic fluids; we refer to them as irreducible CFSDs (ICFSDs). For a proper choice of symmetry-adapted functions, the ICFSDs are real-valued quantities. Since the symmetry-adapted functions are related to the spherical components V_k by a unitary transformation, it follows that the ICFSDs are linear combinations of the CFSDs appearing in equation (3.3). The number, $\mathcal{N}$, of distinct ICFSD functions is given in table 2 for several point groups of relevance for lyotropic liquid crystals [124]. Note that $\mathcal{N}$ equals the number of LFSD functions only in the case of lamellar, hexagonal, and uniaxial nematic phases. Only in these cases can the ICFSDs be identified with the LFSDs for parallel alignment [76, 125]. The complete information content of a spin relaxation study (at a given magnetic field strength) of a liquid crystal thus consists of $3\mathcal{N}$ ICFSDs. To determine these we need to measure three linearly independent spin relaxation rates at $\mathcal{N}$ different orientations of the liquid crystal. (To improve the accuracy, more than $\mathcal{N}$ orientations can, of course, be investigated.) It is important to realize that the ICFSDs constitute entirely model-independent information; the form of the angular functions $F_{k\lambda}(\theta_{LC}, \phi_C)$ in equation (3.4) is fully determined by the point group symmetry of the mesophase.

3.4. *Symmetry and tensor rank*

While the rotational symmetry of a liquid crystal is determined by its point group, the observable manifestations of this symmetry depend on the tensor rank of the observed physical property. Thus, for example, an observable of rank k cannot distinguish among cyclic or dihedral point groups of higher than k-fold rotation symmetry. Furthermore, even-rank observables are unaffected by inversion symmetry.

Table 2. Number, $\mathcal{N}$, of irreducible crystal-frame spectral density functions in mesophases of various point group symmetries [124].

Mesophase	Translational order	Point group	$\mathcal{N}$
Isotropic fluid	—	$\mathscr{K}_h$	1
Uniaxial nematic	—	$\mathscr{D}_{\infty h}$	3
Biaxial nematic	—	$\mathscr{D}_{2h}$	6
Cubic	3D	$\mathscr{O}_h$	2
Rhombohedral	3D	$\mathscr{D}_{3d}$	4
Tetragonal	3D	$\mathscr{D}_4$	4
Orthorhombic	3D	$\mathscr{D}_2$	6
Hexagonal	2D	6mm	3
Rectangular	2D	2mm	6
Oblique	2D	2	9
Lamellar	1D	L_x/mm	3

When a low-rank property is observed, a liquid crystal may thus appear to have a higher symmetry than prescribed by its point group. A few examples will make this clear.

The spectral lineshape from a liquid crystal powder is determined by the second-rank average EFG tensor and hence cannot distinguish between isotropic fluids and cubic mesophases (which both yield isotropic lineshapes), or between lamellar, hexagonal, tetragonal, rhombohedral, and uniaxial nematic mesophases (which all yield uniaxial lineshapes), or between oblique, rectangular, orthorhombic, and biaxial nematic mesophases (which all yield biaxial lineshapes). The situation is analogous to the classification of the (second-rank) moment of inertia tensor of a molecule as a spherical, symmetric, or asymmetric top.

The spin relaxation rates (and the associated spectral densities) are fourth-rank observables since they are of second order in the quadrupole coupling and thus involve products of two components of a second-rank tensor (cf. equation (2.1)). As in the coupling of angular momenta, this product can be decomposed into tensor components of ranks from zero to four [120]. As a consequence, the spin relaxation behaviour (its orientational dependence and the number of ICFSDs) is not the same in cubic mesophases as in isotropic fluids. Lamellar, hexagonal, and uniaxial nematic mesophases all have uniaxial relaxation behaviour, but differ from tetragonal and rhombohedral mesophases (cf. table 2). It is evident from these remarks that the terms isotropic, uniaxial, and biaxial must be used with care when discussing high-rank observables such as spin relaxation rates.

3.5. *Uniaxial relaxation behaviour*

Due to the ubiquity of lamellar, hexagonal, and uniaxial nematic mesophases, the case of uniaxial relaxation behaviour is of particular importance. Since the spherical tensor components V_k transform according to the irreducible representations A_1 ($k=0$), E_1 ($k=\pm 1$), and E_2 ($k=\pm 2$) of the point groups $\mathscr{D}_{\infty h}$ and 6mm, they are already adapted to the symmetry of these mesophases. Consequently, equation (3.4) reduces to equation (3.3). Furthermore, according to the Wigner–Eckart theorem, all off-diagonal terms in equation (3.3) vanish so that

$$J^L_{kk}(k\omega_0;\theta_{LC}) = \sum_{n=0}^{2} (1-\delta_{n0}/2)\{[d^2_{kn}(\theta_{LC})]^2 + [d^2_{k-n}(\theta_{LC})]^2\} J^C_{nn}(k\omega_0). \tag{3.5}$$

As expected, the dependence on the azimuthal angle ϕ_C has disappeared. In this case, a spin relaxation study can yield the nine model-independent quantities $J^C_{nn}(k\omega_0)$, with $k, n = 0, 1, 2$.

4. Connection to microstructure and dynamics

4.1. *Levels of structural organization*

The irreducible crystal-frame spectral density functions and the corresponding time correlation functions reflect the thermal fluctuations of the instantaneous EFG tensor at the nuclear site. In a lyotropic mesophase these fluctuations occur on several length and time scales, corresponding to the different levels of structural organization in the mesophase (cf. §1). In most mesophases, fluctuations on three levels must be considered. At the local level there are fast ($\leqslant 0{\cdot}1$ ns) fluctuations of the instantaneous EFG relative to the local interface. At the microstructural level the orientation of the local interface experienced by the nucleus fluctuates through diffusive processes on intermediate length (1–5 nm) and time (1–10 ns) scales. At the long wavelength level the entire microstructure fluctuates on still larger length and time scales.

4.2. *Time scale decomposition of spectral densities*

Although the overall EFG fluctuations in a lyotropic mesophase are quite complex, involving a wide spectrum of dynamic processes, their gross features can be described in a simple and essentially model-independent way. This is possible because the presence of distinct levels of structural organization implies that fluctuations at different levels occur on distinct time scales and, hence, are statistically uncorrelated. The overall thermal randomization of the EFG can then be seen as a stepwise projection process, where the instantaneous EFG components are projected on to the macroscopic liquid crystal axes via intermediate coordinate frames associated with the local interface and the microstructural elements. Because of their statistical independence, each of these projection steps contributes an independent term to the ICFSDs,

$$J_\lambda^{\mathrm{C}}(k\omega_0) = J_\lambda^{\mathrm{loc}}(k\omega_0) + J_\lambda^{\mathrm{ms}}(k\omega_0) + J_\lambda^{\mathrm{lw}}(k\omega_0). \tag{4.1}$$

The symmetry classification of the individual terms in equation (4.1) is based on the point group symmetry of the macroscopic liquid crystal. Since this symmetry determines the orientation dependence of the LFSDs (cf. § 3), the quantities in equation (4.1) are the experimentally accessible ones. (We assume here that the spin-bearing molecule samples the symmetry of the mesophase on the time scale of spin relaxation.) In certain mesophases, however, the symmetry of the microstructural elements is lower than that of the mesophase. This is the case, for example, for biaxial aggregates in a uniaxial nematic phase [126], for locally biaxial cylinders in a hexagonal phase [19, 22], and for uniaxial aggregates in a micellar cubic phase [127, 128]. In such cases, a group-theoretical analysis based on the point group of the aggregate (or microstructure) should be performed to identify the irreducible aggregate-frame spectral densities $J_\lambda^{\mathrm{ms}}(k\omega_0)$ [124]. The irreducible crystal-frame spectral densities $J_\lambda^{\mathrm{ms}}(k\omega_0)$ in equation (4.1) can then be expressed as linear combinations of the $J_{\lambda'}^{\mathrm{ms}}(k\omega_0)$. The coefficients in these linear combinations depend on the orientational order parameters for the aggregates with respect to the liquid crystal.

We must now ask whether the information accessible by spin relaxation experiments is sufficient to determine the individual contributions from fluctuations at the different levels of structural organization in a lyotropic mesophase. As shown in § 3, relaxation anisotropy experiments at a fixed magnetic field yield $3\mathcal{N}$ ICFSDs (with $\mathcal{N}$ given in table 2), which obviously do not determine the $9\mathcal{N}$ unknown quantities in equation (4.1). Further progress is possible only by considering the time scales of the fluctuations associated with the different terms in equation (4.1).

In most cases of interest, the local motions are fast compared to the Larmor frequency ω_0, i.e. they are in the so-called extreme limit, and thus contribute equally to the adiabatic and non-adiabatic spectral densities,

$$J_\lambda^{\mathrm{loc}}(k\omega_0) = J_\lambda^{\mathrm{loc}}(0). \tag{4.2}$$

At the magnetic field of a conventional NMR spectrometer, the long wavelength motions are usually slow compared to ω_0 and thus contribute only to the adiabatic spectral densities (cf. § 6.3),

$$J_\lambda^{\mathrm{lw}}(k\omega_0) = \delta_{k0} J_\lambda^{\mathrm{lw}}(0). \tag{4.3}$$

If the local fluctuations are sufficiently weakly anisotropic, the dependence on the projection index λ is weak and we may write

$$J_\lambda^{\mathrm{loc}}(0) = J^{\mathrm{loc}}(0). \tag{4.4}$$

This approximation has been directly verified for Na^+ counterions in a hexagonal mesophase [70], and is probably justified also for α-deuteriated single chain surfactants. (In the latter case, the first term in equation (4.1) is usually much smaller than the second term, and therefore contributes little to the observed relaxation anistropy even if equation (4.4) is not strictly valid.)

4.3. *Model-independent analysis of spectral densities*

After introducing the simplifications of equations (4.2)–(4.4) into equation (4.1), we obtain for the non-adiabatic ($k=1,2$) ICFSDs

$$J_\lambda^C(k\omega_0)=J^{loc}(0)+J_\lambda^{ms}(k\omega_0). \tag{4.5}$$

There are now only $2\mathcal{N}+1$ unknown quantities to be determined from the $2\mathcal{N}$ non-adiabatic ICFSDs. There are basically two ways to proceed. One possibility is to introduce a specific microstructural and dynamic model, which, if sufficiently simple, allows the $2\mathcal{N}$ spectral densities $J_\lambda^{ms}(k\omega_0)$ to be expressed in terms of a smaller number of model parameters. An alternative strategy, which is useful if we want to defer introducing a specific microstructural model, is to assume that the spectral densities are lorentzian (i.e. that the corresponding TCFs decay exponentially),

$$J_\lambda^{ms}(k\omega_0)=A_\lambda\frac{\tau_\lambda}{1+(k\omega_0\tau_\lambda)^2}. \tag{4.6}$$

Exact treatments of various specific models show that the lorentzian approximation is sufficiently accurate in many cases [69, 71, 129–134].

By means of equation (4.6), the two quantities $J_\lambda^{ms}(\omega_0)$ and $J_\lambda^{ms}(2\omega_0)$ can be transformed into two new quantities: the fluctuation amplitude A_λ, which is nothing but the initial-value $G_\lambda^{ms}(0)$ of the TCF, and the effective correlation time τ_λ. This transformation has two advantages. First, it separates the spectral density information into a dynamic quantity τ_λ and a static quantity A_λ. The latter is entirely independent of the dynamics and can be calculated with relatively little effort even for quite complex microstructures. Second, the $\mathcal{N}$ fluctuation amplitudes A_λ are, apart from a common factor of proportionality, expressible in terms of $\mathcal{N}-1$ model-independent geometrical parameters [124], which are directly related to the microstructure. The common factor is of the form $\bar{\chi}^2$, where $\bar{\chi}$ is the residual quadrupole coupling constant (averaged by local motions). These quantities provide the link between the spin relaxation data (the ICFSDs) and the quadrupole splitting (cf. § 2), thus giving us a closed algebraïc system of $2\mathcal{N}+1$ experimentally accessible quantities (the $2\mathcal{N}$ non-adiabatic ICFSDs $J_\lambda^C(k\omega_0)$ and the quadrupole splitting) and $2\mathcal{N}+1$ unknowns (the local motion contribution $J^{loc}(0)$, the residual quadrupole coupling constant $\bar{\chi}$, the $\mathcal{N}$ correlation times τ_λ, and the $\mathcal{N}-1$ geometrical parameters). After solving this system, the $\mathcal{N}$ long wavelength contributions $J_\lambda^{lw}(0)$ can be obtained by difference (using equation (4.6)) from the $\mathcal{N}$ adiabatic ICFSDs $J_\lambda^C(0)$. This essentially model-independent interpretational strategy is illustrated in section 7.1 for the case of a lamellar mesophase with intrinsic microstructural defects.

If the local interface normal is at least a threefold axis, the $\mathcal{N}-1$ geometrical parameters can be chosen as the irreducible orientational order parameters of rank $\leqslant 4$ [135] for the microstructure. If the local symmetry is lower, the geometrical parameters are linear combinations of microstructural order parameters weighted by local (molecular) order parameters [124]. In either case, the geometrical parameters are invariant under isometric scaling of the microstructure. The absolute dimensions of the

microstructure can, however, be obtained from the correlation times τ_λ, which are proportional to a^2/D_S, where a is a characteristic length scale in the microstructure and D_S is the surface diffusion coefficient.

4.4. *Relaxation dispersion*

So far we have only considered data derived from spin relaxation studies at a single magnetic field strength B_0. Field-variable relaxation studies provide information about the relaxation dispersion, i.e. the dependence of the spectral densities on the Larmor frequency $\omega_0 = \gamma B_0$. Whereas the relaxation anisotropy allows symmetry selection, i.e. separation of different relaxation contributions on the basis of the rotational symmetry of the dynamic processes, the relaxation dispersion allows frequency selection, i.e. separation of different relaxation contributions on the basis of the time scale of the dynamic processes. Even a fixed field relaxation study affords some frequency selection, of course, since it probes the spectral density functions at three frequencies (0, ω_0, and $2\omega_0$). Field-variable relaxation studies can give a more complete characterization of the spectral density functions. In contrast to the relaxation anisotropy, however, the relaxation dispersion cannot be analysed without recourse to a dynamic model. The ultimate spin relaxation study, comprising relaxation anistropy as well as relaxation dispersion and yielding the frequency dependence of the $\mathcal{N}$ individual ICFSDs, has, to our knowledge, not been conducted on any anisotropic fluid system. As regards lyotropic liquid crystals, relaxation dispersion measurements are particularly valuable for studies of nematic phases, which do not allow conventional relaxation anisotropy measurements (cf. § 3.1). Whereas conventional NMR spectrometers equipped with field-variable magnets allow Larmor frequency variations over a decade or so, several decades can be covered by field cycling techniques. Although subject to other limitations (cf. § 2.4), field cycling dispersion experiments on macroscopically oriented mesophases can give a more complete picture of long wavelength fluctuations (cf. § 6), such as director fluctuations [48].

5. Diffusion on curved surfaces

The information about the microstructure of a lyotropic mesophase is essentially contained in the contributions $J_\lambda^{ms}(k\omega_0)$ to the ICFSDs in equation (4.1). These spectral densities can involve two kinds of dynamic process: (i) translational diffusion of the spin-bearing molecule with respect to the interface, and (ii) reorientational motion of the interface. The latter process is important only in mesophases built from small surfactant aggregates, such as (most) nematic and (some) cubic mesophases. Usually the aggregates exhibit a high degree of orientational order, in which case approximate analytical solutions to the restricted rotational diffusion model can be used [129–132].

For spin-bearing species that are strongly accumulated at or near the interface, such as surfactant molecules and counterions (in the absence of added electrolyte), the diffusion space is effectively reduced to two dimensions, i.e. the translational motion of these species can be treated as a surface diffusion process. If the interface is curved, surface diffusion induces fluctuations in the orientation of the residual (averaged by local motions) EFG tensor, whose symmetry axis usually coincides with the local interface normal. This is the principal mechanism for conveying information about mesophase microstructure to the spin system. For counterions, longitudinal diffusion (along the interface normal) also occurs to some extent. Except in the trivial case of a planar interface, longitudinal and transverse (surface) diffusion are non-separable.

However, detailed studies of the 3D ion diffusion problem in various geometries [136–138], shows that the effect of longitudinal diffusion is usually insignificant [68, 69, 71] (cf. §§ 7.1 and 7.2).

The spectral densities $J_\lambda^{sd}(k\omega_0)$ can be calculated for diffusion on any well-defined surface of prescribed geometry. (The case of fluctuating surfaces is discussed in section 6.) The associated TCF can be expressed in terms of the curvilinear surface coordinates (u, v) as [133]

$$G_\lambda^{sd}(\tau) = \int du_0 \int dv_0 \; [g(u_0, v_0)]^{1/2} f_{eq}(u_0, v_0) [\bar{V}_\lambda(u_0, v_0) - \langle \bar{V}_\lambda \rangle]^* \times \int du \int dv [g(u, v)]^{1/2} f[(u, v, \tau | u_0, v_0)[\bar{V}_\lambda(u, v) - \langle \bar{V}_\lambda \rangle], \tag{5.1}$$

where $\bar{V}_\lambda$ is a symmetry-adapted residual EFG component in a surface-fixed frame, $g(u, v)$ is the determinant of the metric tensor, $f_{eq}(u, v)$ is the equilibrium surface distribution of the spin-bearing species, and the propagator $f(u, v, \tau | u_0, v_0)$ satisfies the generalized surface diffusion equation [139]

$$\frac{\partial}{\partial \tau} f(u, v, \tau | u_0, v_0) = \nabla_S \cdot D_S(u, v) \cdot [f_{eq}(u, v) \nabla_S f(u, v, \tau | u_0, v_0) / f_{eq}(u, v)], \tag{5.2}$$

and the initial condition

$$f(u, v, 0 | u_0, v_0) = \delta(u - u_0)\delta(v - v_0)/[g(u_0, v_0)]^{1/2}. \tag{5.3}$$

Rather than pursuing the general case, we shall consider the surface diffusion problem under certain simplifying assumptions, which are justified in most cases of interest. The spin-bearing species is taken to be uniformly distributed over the surface (of area A_S), i.e.

$$f_{eq}(u, v) = \frac{1}{A_S}, \tag{5.4}$$

and its diffusion tensor is taken to be uniform and isotropic in the surface, i.e.

$$\mathbf{D}_S(u, v) = D_S \mathbf{I}. \tag{5.5}$$

Furthermore, we restrict attention to centrosymmetric surfaces of revolution (point group $\mathscr{D}_{\infty h}$) with approximately threefold site symmetry, whence

$$\bar{V}_\lambda(u, v) - \langle \bar{V}_\lambda \rangle = \bar{V}_S[d_{m0}^2(\theta) \exp(-im\phi) - \delta_{m0}\langle d_{00}^2 \rangle], \tag{5.6}$$

where θ and ϕ are the spherical polar angles for the orientation of the local surface normal, and $\bar{V}_S$ is the principal residual EFG component in a local frame. $\bar{V}_S$ is proportional to the residual quadrupole coupling constant $\bar{\chi}$ and is taken to be uniform over the interface.

After these simplifications, equation (5.1) can be expressed as [133]

$$G_{nn}^{sd}(\tau) = \frac{\bar{V}_S^2}{\alpha} \int d\eta_0 h(\eta_0) \hat{d}_{n0}^2(\theta_0) \int d\eta h(\eta) f_n(\eta, \tau | \eta_0) \hat{d}_{n0}^2(\theta), \tag{5.7}$$

where η is a dimensionless surface coordinate orthogonal to ϕ, $h(\eta) = [g(\eta, \phi)]^{1/2}/a^2$ is a dimensionless metric factor, $\alpha = A_S/a^2$ is the reduced surface area, a is a length

characteristic of the surface, and $\hat{d}^2_{n0}(\theta) = d^2_{n0}(\theta) - \delta_{n0}\langle d^2_{00}\rangle$, with $\theta = \theta(\eta)$. The modified propagator $f_n(\eta, \tau|\eta_0)$ satisfies

$$\frac{\partial}{\partial\tau} f_n(\eta, \tau|\eta_0) = -\frac{D_S}{h(\eta)} \mathscr{L}_n f_n(\eta, \tau|\eta_0), \tag{5.8}$$

where $\mathscr{L}_n$ is the self-adjoint second order differential operator

$$\mathscr{L}_n = h(\eta)[n^2 - a^2\nabla^2_\eta], \tag{5.9}$$

with ∇^2_η being the η-part of the surface laplacian.

To calculate the spectral density functions

$$J^{sd}_{nn}(\omega) = \int_0^\infty d\tau \cos(\omega\tau) G^{sd}_{nn}(\tau), \tag{5.10}$$

we have to solve the partial differential equation (5.8), perform the integrations in equation (5.7), and take the cosine transform in equation (5.10). It can be shown, however, that the same result can be obtained more easily by performing a single integral,

$$J^{sd}_{nn}(\omega) = \bar{V}^2_S \frac{a^2}{D_S} \int d\eta h(\eta) \hat{d}^2_{n0}(\theta) \operatorname{Re}[Q_n(\eta, \omega)], \tag{5.11}$$

where the quantity $Q_n(\eta, \omega)$ satisfies the ordinary differential equation

$$\left[\frac{1}{h(\eta)} \mathscr{L}_n - i\frac{a^2}{D_S}\omega\right] Q_n(\eta, \omega) = \hat{d}^2_{n0}(\theta). \tag{5.12}$$

This direct approach has two important advantages [133]. First, its numerical implementation is highly efficient, simply involving the solution of the (complex) matrix equation resulting from equation (5.12) after discretizing the η coordinate and approximating derivatives by finite differences. Second, it often allows the adiabatic spectral densities $J^{sd}_{nn}(0)$ to be obtained by simple quadrature, sometimes even analytically. A case in point is the truncated catenoid of inner radius a and height $2b$ (a plausible model for pore defects in bilayers, cf. § 7.1), for which

$$J^{sd}_{22}(0) = \bar{V}^2_S \frac{3a^2}{16D_S}\left[1 + \frac{a}{2b}\sinh\left(\frac{2b}{a}\right)\right]^{-1}. \tag{5.13}$$

In the limit $b/a \to \infty$, the truncated catenoid degenerates into a cylinder of radius a and equation (5.13) reduces to

$$J^{sd}_{22}(0) = \bar{V}^2_S \frac{3a^2}{32D_S}. \tag{5.14}$$

For a prolate spheroid of minor and major semi-axes a and b, with $b \gg a$,

$$J^{sd}_{22}(0) = \bar{V}^2_S \frac{9a^2}{128D_S}, \tag{5.15}$$

which is 3/4 of the cylinder result in equation (5.14). Another simple case is the oblate spheroid with $b \gg a$, for which

$$J^{sd}_{11}(0) = \bar{V}^2_S \frac{a^2}{12D_S}, \tag{5.16}$$

which is a factor 5/2 larger than the result for a sphere of radius a.

The spectral densities for diffusion on spherical and cylindrical surfaces are strictly lorentzian. For a sphere of radius a,

$$J_{nn}^{sd}(\omega)=\tfrac{1}{5}\overline{V}_S^2\frac{\tau_S}{1+(\omega\tau_S)^2},\qquad \tau_S=\frac{a^2}{6D_S}, \tag{5.17}$$

and for a cylinder of radius a,

$$J_{nn}^{sd}(\omega)=\delta_{n2}\tfrac{3}{8}\overline{V}_S^2\frac{\tau_S}{1+(\omega\tau_S)^2},\qquad \tau_S=\frac{a^2}{4D_S}. \tag{5.18}$$

6. Long wavelength fluctuations

6.1. *Continuum description*

When discussing the microstructure of a lyotropic liquid crystal, we usually refer to an idealized ground state configuration. Like any other condensed phase, however, a lyotropic mesophase is subject to thermal fluctuations and these will influence its microstructure. Although quadrupolar spin relaxation probes single-particle reorientational dynamics, it may be profoundly affected by collective fluctuations in fluids where the orientational correlation length substantially exceeds molecular dimensions. If this correlation length is effectively infinite, as in liquid crystals, collective fluctuation modes on a wide range of length scales may affect the spin relaxation.

Collective fluctuations in liquid crystals are usually analysed within the framework of continuum mechanics (elasticity theory and hydrodynamics). The equilibrium description then involves certain macroscopic material constants, components of the fourth-rank elastic modulus tensor, that determine the free energy of isothermal deformation of the liquid crystal [140]. The material constants of uniaxial liquid crystals are the splay, twist, and bend elastic moduli K_1, K_2, and K_3, the bulk modulus (osmotic compressibility) B, and the shear modulus μ. In addition, the hydrodynamic description involves a number of viscosity coefficients [141] (5 for a uniaxial mesophase).

The continuum description of a lyotropic liquid crystal is valid only on length scales that are large compared to the dimensions of its microstructure. Spin relaxation, however, probes the liquid crystal at a molecular level. We therefore face the problem of accounting, in a self-consistent manner, for the spin relaxation contributions from molecular processes, described by microscopic models, and for contributions from collective processes, described by continuum theory. This is a fundamental statistical-mechanical problem that appears in many guises throughout condensed matter physics. Our problem is thus to divide the fluctuation spectrum between the two ICFSD terms $J_\lambda^{ms}(k\omega_0)$ and $J_\lambda^{lw}(k\omega_0)$ in equation (4.4) in such a way that $J_\lambda^{ms}(k\omega_0)$ accounts for short wavelength fluctuations, describable in terms of the (ground state) microstructure, while $J_\lambda^{lw}(k\omega_0)$ accounts for long wavelength fluctuations, describable in terms of the macroscopic (zero wavenumber) material constants of the mesophase. The conventional solution to this problem is to introduce a short wavelength cut off [25], above which the continuum description is taken to be valid, and to hope that the microscopic model for $J_\lambda^{ms}(k\omega_0)$ takes care of fluctuations at shorter wavelengths. To avoid this somewhat artificial division into short wavelength and long wavelength fluctuation modes we would need an entirely microscopic description in terms of aggregate size and shape and interaggregate forces, which is not available at present.

6.2. *Time correlation functions*

Since the long wavelength fluctuations in lyotropic liquid crystals are generally of small amplitude, they contribute significantly to the spin relaxation only if they are

slow. At conventional magnetic fields this means, as noted in § 4.2, that we only need to consider the adiabatic spectral densities $J^{\mathrm{lw}}_{\lambda}(0)$ [72, 73]. (We disregard critical fluctuations occurring in the vicinity of phase transitions [25, 125, 142–144].)

The qualitative features of long wavelength fluctuations in liquid crystals are determined by the point group symmetry of the mesophase and the dimensionality of the long range translational order. In the following, we restrict our attention to the 'uniaxial' case, i.e. lamellar, hexagonal, and uniaxial nematic mesophases (cf. § 3), with three distinct ICFSDs: $J^{\mathrm{lw}}_{nn}(0)$, $n=0,1,2$. If the uniaxial symmetry of the mesophase persists at the local level (down to the short wavelength cut off), the effect of long wavelength fluctuations on the spin relaxation can be described in terms of a unit vector field $\mathbf{n}(\mathbf{r})$, referred to as the local director. The local director should be understood in a 'coarse-grained' sense; it refers to a volume of linear dimensions comparable to the short wavelength cut off. The average $\mathbf{n}_0=\langle\mathbf{n}(\mathbf{r})\rangle$, taken over the liquid crystal, coincides with the macroscopic symmetry axis of the uniaxial mesophase.

The adiabatic spectral densities $J^{\mathrm{lw}}_{nn}(0)$ are the time integrals of the corresponding TCFs $G^{\mathrm{lw}}_{nn}(\tau)$, which can be expressed in terms of the local director components $n_{\pm}=n_x \pm \mathrm{i}\, n_y$ as [73, 145]

$$G^{\mathrm{lw}}_{00}(\tau)=\tfrac{9}{4}\bar{V}_0^2[\langle|n_+(0)|^2|n_+(\tau)|^2\rangle-\langle|n_+|^2\rangle^2], \tag{6.1 a}$$

$$G^{\mathrm{lw}}_{11}(\tau)=\tfrac{3}{2}\bar{V}_0^2\langle n_+(0)n_-(\tau)\rangle+\mathcal{O}(n_{\pm}^4), \tag{6.1 b}$$

$$G^{\mathrm{lw}}_{22}(\tau)=\tfrac{3}{8}\bar{V}_0^2\langle n_+^2(0)n_-^2(\tau)\rangle. \tag{6.1 c}$$

It is seen that $G^{\mathrm{lw}}_{00}(\tau)$ and $G^{\mathrm{lw}}_{22}(\tau)$ are of fourth order in the fluctuating director components n_x and n_y, whereas the leading contribution to $G^{\mathrm{lw}}_{11}(\tau)$ is of second order.

The second-rank orientational order parameter associated with long wavelength fluctuations in a uniaxial phase is given by [25]

$$S_{\mathrm{lw}}=\langle P_2(\mathbf{n}\cdot\mathbf{n}_0)\rangle=1-3\langle n_x^2\rangle. \tag{6.2}$$

If all fluctuation modes are fast compared to the inverse of the quadrupole coupling fluctuations which they induce, the quadrupole splitting is proportional to S_{lw}.

According to the standard continuum theory of fluctuations in uniaxial liquid crystals, which is restricted to small fluctuations (thus excluding critical phenomena), the free energy of isothermal deformation can be expressed, to second order in the local director components, as the Fourier expansion [25, 140]

$$F=\frac{1}{2V}\sum_{\mathbf{q}}[\phi_1(\mathbf{q})|\hat{\mathbf{n}}_1(\mathbf{q})|^2+\phi_2(\mathbf{q})|\hat{\mathbf{n}}_2(\mathbf{q})|^2], \tag{6.3}$$

where $\hat{\mathbf{n}}_1(\mathbf{q})$ and $\hat{\mathbf{n}}_2(\mathbf{q})$ are the independent fluctuation eigenmodes that diagonalize the quadratic form in equation (6.3), and the associated potential functions $\phi_1(\mathbf{q})$ and $\phi_2(\mathbf{q})$ contain the moduli of the mesophase. Application of the equipartition theorem to equation (6.3) leads directly to the mean square fluctuation amplitudes

$$\langle|\hat{\mathbf{n}}_{\alpha}(\mathbf{q})|^2\rangle=\frac{k_{\mathrm{B}}TV}{\phi_{\alpha}(\mathbf{q})}, \qquad \alpha=1,2. \tag{6.4}$$

These can then be used to express the order parameter S_{lw} and the initial TCFs $G^{\mathrm{lw}}_{nn}(0)$ in terms of the moduli. The TCFs involve fourth order averages, which, however, are simply related to the second order averages since the quadratic form of the free energy ensures that the director components are gaussian random variables [139]. Within the

second order fluctuation theory, the initial TCFs are simply related to the order parameter S_{lw} [73],

$$G_{00}^{lw}(0) = 3G_{22}^{lw}(0) = (1 - S_{lw})^2, \tag{6.5 a}$$

$$G_{11}^{lw}(0) = 1 - S_{lw}. \tag{6.5 b}$$

As noted in § 3.4, the TCFs are fourth-rank quantities, and their initial values should therefore, for uniaxial mesophases, involve also the fourth-rank order parameter $Q_{lw} = \langle P_4(\mathbf{n}\cdot\mathbf{n}_0)\rangle$. However, the harmonic approximation underlying equation (6.3) implies a definite relationship between Q_{lw} and S_{lw}.

In general, the director components $n_\pm(\tau)$ in equation (6.1) fluctuate in time as a result of two distinct dynamical processes: (i) translational diffusion of the spin-bearing molecule through the inhomogeneous director field, i.e. $n_\pm(\tau) = n_\pm(\mathbf{r}(\tau))$, and (ii) collective fluctuations of the orientation of the local director at a given 'point', i.e. $n_\pm(\tau) = n_\pm(\mathbf{r}, \tau)$. If one of these processes is much faster, the other one has no effect. We now discuss the two possible limiting cases.

6.3. *Translational diffusion in a static director field*

If translational diffusion is much faster than director fluctuations the diffusing spin will see an effectively static director field, and the TCFs in equation (6.1) can be expressed as [73] (omitting the common factor $\bar{V}_0^2$)

$$G_{00}^{lw}(\tau) = \tfrac{9}{4} \int d\mathbf{r}\, f(\mathbf{r}, \tau)[\langle |n_+(0)|^2 |n_+(\mathbf{r})|^2 \rangle - \langle |n_+|^2 \rangle^2], \tag{6.6 a}$$

$$G_{11}^{lw}(\tau) = \tfrac{3}{2} \int d\mathbf{r}\, f(\mathbf{r}, \tau) \langle n_+(0) n_-(\mathbf{r}) \rangle, \tag{6.6 b}$$

$$G_{22}^{lw}(\tau) = \tfrac{3}{8} \int d\mathbf{r}\, f(\mathbf{r}, \tau) \langle n_+^2(0) n_-^2(\mathbf{r}) \rangle. \tag{6.6 c}$$

Here $f(\mathbf{r}, \tau)$ is the propagator for (anisotropic) translational diffusion of the spin-bearing species through the liquid crystal. Due to the translational invariance (on the 'coarse-grained' scale), there is no dependence on the initial position (i.e. we can set $\mathbf{r} = 0$ at $\tau = 0$). It is interesting to note that the director components $n_{x,y}(\tau) = n_{x,y}(\mathbf{r}(\tau))$ are stochastic at two levels since they represent a random motion $[\mathbf{r}(\tau)]$ in a random medium $[n_{x,y}(\mathbf{r})]$. The composite stochastic processes $n_{x,y}(\tau)$ are in general non-markovian.

The quantities within angular brackets in equations (6.6) are spatial correlation functions of the gaussian random variables $n_\pm(\mathbf{r})$. Using the gaussian property, it is readily shown that [73, 145]

$$\langle |n_+(0)|^2 |n_+(\mathbf{r})|^2 \rangle - \langle |n_+|^2 \rangle^2 = \tfrac{1}{2} \langle n_+^2(0) n_-^2(\mathbf{r}) \rangle, \tag{6.7}$$

whence

$$G_{00}^{lw}(\tau) = 3G_{22}^{lw}(\tau). \tag{6.8}$$

This result is simply a consequence of the small amplitude of the orientational fluctuations, implied by the quadratic form of the hamiltonian in equation (6.3). The relation $J_{00}^{lw}(0) = 3J_{22}^{lw}(0)$, which follows trivially from equation (6.8), provides a useful check in the data analysis.

The two distinct TCFs may be expressed in terms of the mean square mode amplitudes $\langle|n_+(\mathbf{q})|^2\rangle$, simply related to those in equation (6.4), as

$$G_{00}^{\mathrm{lw}}(\tau)=\tfrac{9}{4}(2\pi)^{-6}V^{-2}\int d\mathbf{q}\int d\mathbf{q}'\langle|n_+(\mathbf{q})|^2\rangle\langle|n_+(\mathbf{q}')|^2\rangle$$
$$\times\exp\{-[|\mathbf{q}_\perp+\mathbf{q}'_\perp|^2D_\perp+(q_Z-q'_Z)^2D_\parallel]\tau\}, \tag{6.9 a}$$

$$G_{11}^{\mathrm{lw}}(\tau)=\frac{3}{2V}\int d\mathbf{q}\langle|n_+(\mathbf{q})|^2\rangle\exp[-(q_\perp^2D_\perp+q_z^2D_\parallel)\tau]. \tag{6.9 b}$$

The longitudinal (along the mean director) and transverse (perpendicular to the mean director) diffusion coefficients $D_\parallel$ and $D_\perp$ in equations (6.9) are the macroscopic (zero wave vector) quantities that are measured, for example, in a pulsed field gradient NMR experiment (cf. § 1). They are thus averaged over the microstructure and may differ by orders of magnitude from the surface diffusion coefficient D_S introduced in § 5.

The adiabatic spectral densities $J_{nn}^{\mathrm{lw}}(0)$ are obtained from equations (6.9) after a trivial integration over τ and a somewhat less trivial wavevector integration. To avoid divergences, it is generally necessary to include in the free energy in equation (6.3) the interaction of the static magnetic field with the anisotropic diamagnetic susceptibility of the mesophase. This introduces a new length scale, the magnetic coherence length, which acts as a long wavelength cut off.

For a (non-polymer) nematic mesophase, neglecting the anisotropy (which should be relatively small in lyotropic nematics) in the diffusivity and elasticity tensors, we find [73]

$$J_{00}^{\mathrm{lw}}(0)=3J_{22}^{\mathrm{lw}}(0)=\left(\frac{3k_BT}{\pi K}\right)^2\frac{1}{16D}[\ln(1/\varepsilon)-1{\cdot}12+\mathcal{O}(\varepsilon)], \tag{6.10 a}$$

$$J_{11}^{\mathrm{lw}}(0)=\frac{3k_BT}{\pi K}\frac{\xi_m}{D}\left[1-\frac{2}{\pi}\varepsilon+\mathcal{O}(\varepsilon^3)\right], \tag{6.10 b}$$

with $\varepsilon=\lambda_c/(2\pi\xi_m)$, where λ_c is the short wavelength cut off and ξ_m is the magnetic coherence length [25, 73],

$$\xi_m=\left[\frac{\mu_0KS_{\mathrm{lw}}}{(\chi_\parallel^C-\chi_\perp^C)P_2(\cos\theta_{LC})}\right]^{1/2}\frac{1}{B_0}, \tag{6.11}$$

where $\chi_\parallel^C$ and $\chi_\perp^C$ are diamagnetic susceptibility components in the liquid crystal frame. For lyotropic nematics in conventional magnetic fields, ξ_m is of the order 10^{-5} m.

It was stated in §3.2 that the intrinsic properties of a liquid crystal do not depend significantly on its orientation with respect to the magnetic field. This is not quite true since, according to equation (6.11), the magnetic coherence length ξ_m, which sets the range for spatial correlations of the fluctuating local director components $n_{x,y}(\mathbf{r})$ [25], depends on the crystal orientation θ_{LC}. This leads to a significant θ_{LC} dependence in $J_{11}^{\mathrm{lw}}(0)$, which causes a departure from the orientation dependence of the adiabatic LFSD predicted by equation (3.5).

The results in equation (6.10) should be generally valid for counterion nuclei in lyotropic nematics, since the counterion diffusion coefficient D is typically two orders of magnitude larger than the director fluctuation diffusion coefficient K/η so that the director field can be treated as static. A welcome feature of the result in equation (6.10 *a*) is the very weak dependence of $J_{00}^{\mathrm{lw}}(0)$ on the imprecisely defined short wave length cut off λ_c. Given an independent determination (or estimate) of D, spin relaxation

data can thus be used to determine the effective elasticity modulus K. The spectral density $J^{lw}_{11}(0)$ cannot be measured for nematic mesophases without special alignment techniques (cf. § 3.1). On the basis of equation (6.10) and a typical $K = 1$ pN, we expect $J^{lw}_{11}(0)$ to be at least 5 orders of magnitude larger than $J^{lw}_{00}(0)$, calling into question the validity of the motional narrowing approximation in the conventional spin relaxation theory [82]. In contrast, the non-adiabatic spectral density $J^{lw}_{11}(0)$, which could easily be measured, does not contribute significantly to the spin relaxation in lyotropic nematics at conventional magnetic fields [73]. Under these conditions [73, 146]

$$J^{lw}_{11}(\omega_0) = \frac{4\pi k_B T D}{K \lambda_c^3} \frac{1}{\omega_0^2}. \tag{6.12}$$

Even if $J^{lw}_{11}(\omega_0)$ did make a significant contribution, it would not be of much value due to the strong λ_c dependence.

Whereas the surface diffusion coefficient D_S is often of comparable magnitude for counterions and (single chain) surfactants [69], the bulk diffusion coefficient D in nematic phases may be several orders of magnitude smaller for surfactants than for counterions. Since the surfactant has to jump from one aggregate to another, its macroscopic diffusion coefficient is determined by its mean residence time in an aggregate (*c.* 10^{-5} s for a C_{12} chain). Consequently, the static director limit is not applicable to surfactants in nematic phases. In a lamellar phase, this limit may be applicable for counterions as well as for surfactants in the transverse plane, but not in the longitudinal direction (unless the lamellae have perforation defects). In a hexagonal phase the situation is reversed with relatively fast diffusion in the longitudinal direction, but with slow diffusion in the transverse plane. In these translationally ordered phases spin relaxation studies might provide valuable information about surface forces via the dependence of $J^{lw}_{nn}(0)$ on the osmotic compressibility [147–149].

6.4. *Immobile spin subject to director fluctuations*

When the static director limit is not applicable, the hydrodynamics of director fluctuations must be considered [25]. In the case of nematic phases (neglecting anisotropies), the result [125, 150, 151] is simple for the second order TCF $G^{lw}_{11}(\tau)$ and its associated spectral density: we simply replace D in the result for a static director field with $D + K/\eta$. For the fourth order TCFs $G^{lw}_{00}(\tau)$ and $G^{lw}_{22}(\tau)$, the basic problem is that they cannot be obtained from a second order theory. (In the static director limit, this problem does not arise since the static director component distribution is gaussian.) We are then forced to make the additional assumption that the different wavevector components of the director field behave as independent gaussian Markov processes [145, 152]. Proceeding in this way, we find for a nematic phase (neglecting anisotropies), in the immobile spin limit ($D \ll K/\eta$) [73],

$$J^{lw}_{00}(0) = 3J^{lw}_{22}(0) = \frac{(3k_B T)^2 \eta}{(2\pi K)^3} [\ln(1/\varepsilon) - 1{\cdot}52 + \mathcal{O}(\varepsilon)]. \tag{6.13}$$

It should be noted that this result is not obtained from equation (6.10 *a*) by replacing D with K/η.

7. Applications

In the preceding sections we have presented a rather general discussion of quadrupolar spin relaxation in lyotropic liquid crystals. To illustrate the general principles, we devote this section to a more specific discussion of spin relaxation in the most commonly occurring mesophases. These examples, taken from our recent and

current work, are intended to give an appreciation of the potential and limitations of spin relaxation experiments for studying microstructure and dynamics in lyotropic liquid crystals.

7.1. *The lamellar phase*

The lamellar phase is the only lyotropic smectic mesophase with complete lateral disorder. Since the lamellar phase is built from planar interfaces, we expect relaxation contributions from local motions and long wavelength smectic undulation modes (the first and third terms in equation (4.1)), but not from surface diffusion. Under the assumptions of equations (4.2)–(4.4), we therefore expect that all the six non-adiabatic ICFSDs should be equal,

$$J^{\mathrm{C}}_{nn}(k\omega_0) = J^{\mathrm{loc}}(0).$$

Actually, there is also a contribution to the secular ICFSD $J^{\mathrm{C}}_{00}(k\omega_0)$ from fluctuations in the magnitude of the residual EFG (averaged by local motions) due to translational diffusion of the spin-bearing species along the interface normal [136, 137]. Since the residual EFG is non-zero only in the locally anisotropic interface region (of width δ), it may be modelled as a step function. The effective correlation time is then of the order δ^2/D_{N}, where D_{N} is the diffusion coefficient in the normal direction. At conventional magnetic fields this is much smaller than the Larmor period $1/\omega_0$, whence equation (7.1) becomes

$$J^{\mathrm{C}}_{nn}(k\omega_0) = J^{\mathrm{loc}}(0) + \delta_{n0} J^{\mathrm{nd}}_{00}(0), \tag{7.2}$$

with an adiabatic 'normal diffusion' contribution of the form [137]

$$J^{\mathrm{nd}}_{00}(0) = \bar{V}^2_{\mathrm{A}} f(1-f)[(1-f)\tau_{\mathrm{A}} + f\tau_{\mathrm{B}}], \tag{7.3}$$

where τ_{A} is the mean residence time for the fraction f of the nuclei in the anisotropic interface region and τ_{B} is the mean residence time for the fraction $1-f$ of the nuclei in the remaining, essentially isotropic, bulk-like region. These residence times can be obtained by quadrature for any spatial distribution function [137]. (Note that the detailed balance relation $f\tau_{\mathrm{B}} = (1-f)\tau_{\mathrm{A}}$ is not valid in a continuous diffusion description.)

For counterions (in the absence of added electrolyte), the full spectral density function $J^{\mathrm{nd}}_{00}(\omega)$ can be calculated analytically [136, 153]. Usually, however, we only need the adiabatic contribution, which under most conditions is given by [136]

$$J^{\mathrm{nd}}_{00}(0) = \bar{V}^2_{\mathrm{A}} \frac{\delta^2}{4D_{\mathrm{N}}} \frac{\lambda_{\mathrm{GC}} d}{(\delta + \lambda_{\mathrm{GC}})^2}. \tag{7.4}$$

This simple result is valid if the Gouy–Chapman length $\lambda_{\mathrm{GC}} = 2\varepsilon_0\varepsilon_{\mathrm{r}} k_{\mathrm{B}} T/|ze\sigma|$ (typically a few Ångstrom) is much smaller than the thickness d of the aqueous layer. This contribution is important only for water-swollen lamellar phases ($d \geqslant 3$ nm) in the absence of added electrolyte.

In recent years it has become clear that the microstructure of lamellar phases sometimes deviates markedly from the classical picture of continuous planar surfactant bilayers of indefinite lateral extent [15–24]. The bilayers may, for example, be perforated by aqueous pores or slits or may even be fragmented, forming layers of discoidal aggregates. Since such intrinsic structural defects necessarily introduce curvature, they should be manifested in the spin relaxation behaviour. The spin relaxation method is particularly attractive here since it is a null experiment: provided

that equations (4.2)–(4.4) are valid and there is no signifcant contribution from normal diffusion, the two non-adiabatic LFSDs $J^{L}_{11}(\omega_0)$ and $J^{L}_{22}(2\omega_0)$ should be equal and independent of orientation for a classical lamellar phase. In the presence of defects, however, the non-zero contributions $J^{ms}_{nn}(k\omega_0)$ will give rise to a relaxation anisotropy as well as a frequency dependence.

We now consider the ^{23}Na relaxation data obtained from the counterions in a homeotropically aligned sample of the lamellar phase in the system sodium dodecyl sulphate/water/decanol [71]. We know from studies of the hexagonal phase [70] that equations (4.2)–(4.4) are valid (cf. § 7.2). Figure 1 (*a*) shows the orientation dependence of the non-adiabatic LFSDs: the microstructure is clearly non-classical. The six non-adiabatic ICFSDs resulting from fits of equation (3.5) are shown in figure 1 (*b*).

A model-independent analysis, based on equations (4.5) and (4.6), of the six non-adiabatic ICFSDs and the quadrupole splitting yields the local motion contribution

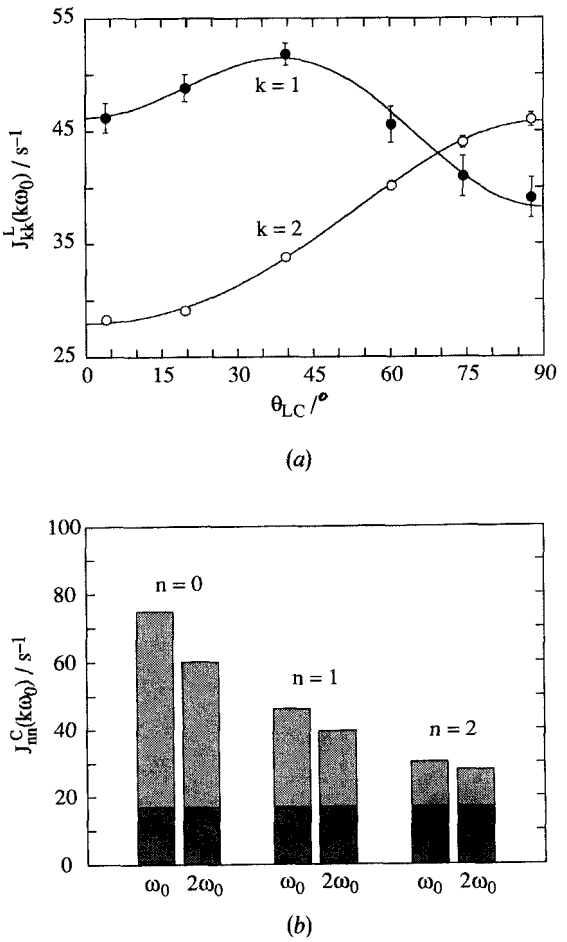

Figure 1. ^{23}Na relaxation data from counterions in the lamellar phase of the system sodium dodecyl sulphate/water/decanol [71]. (*a*) Variation of the non-adiabatic lab-frame spectral densities with the crystal orientation, θ_{LC}. (*b*) Crystal-frame spectral densities derived, according to equation (3.5), from the fits in (*a*). The dark area represents the local motion contribution $J^{loc}(0)$.

$J^{loc}(0)$, shown in figure 1 (*b*), the residual quadrupole coupling constant $\bar{\chi}$, the three correlation times τ_0, τ_1, and τ_2, and two geometrical parameters which we define as

$$\sigma_2 = \langle \sin^2 \theta_{CN} \rangle, \tag{7.5a}$$

$$\sigma_4 = \langle \sin^4 \theta_{CN} \rangle, \tag{7.5b}$$

where θ_{CN} is the angle between the local interface normal and the symmetry axis of the phase, and the angular brackets denote an average over the distribution $f(\theta_{CN})$ of local interface normal orientations. Since $\sigma_2 = \sigma_4 = 0$ for a planar interface, we can write

$$\sigma_k = P\hat{\sigma}_k, \tag{7.6}$$

where P is the fraction of counterions associated with curved interfaces (i.e. defects) and $\hat{\sigma}_k$ refers to the defect. The ratio $\sigma_2/\sigma_4 = \hat{\sigma}_2/\hat{\sigma}_4$ thus characterizes the defect and, if the counterion distribution is laterally uniform within the defect, it directly reflects the defect geometry. The experimental result is $\sigma_2/\sigma_4 = 1{\cdot}48 \pm 0{\cdot}06$.

We consider four types of bilayer defect: hemitoroidal and (truncated) catenoidal pores, a cylindrical slit (or ribbon), and a completely fragmented bilayer composed of oblate spheroids. For these defect models, the distribution function $\hat{f}(\theta_{CN})$ depends on a single parameter $\lambda = b/a$, where $2b$ is the bilayer thickness and $2a$ the pore diameter, ribbon width, or oblate diameter. All defect models, such as cylindrical pores or rectangular slits, that only introduce interfaces with $\theta_{CN} = \pi/2$ can be discarded since they predict that $J_{11}^{ms}(\omega) = 0$, and hence cannot account for the ICFSDs $J_{11}^{C}(\omega_0)$ and $J_{11}^{C}(2\omega_0)$ in figure 1 (*b*).

Calculating $\hat{\sigma}_2/\hat{\sigma}_4$ as a function of λ for the four defect models and comparing with the experimental result, we see, in figure 2, that the data are consistent with three of the models, but only within certain ranges of λ. By considering the individual σ_2 and σ_4 values, the oblate model (for which $P = 1$) can be discarded. (This is true even if we allow

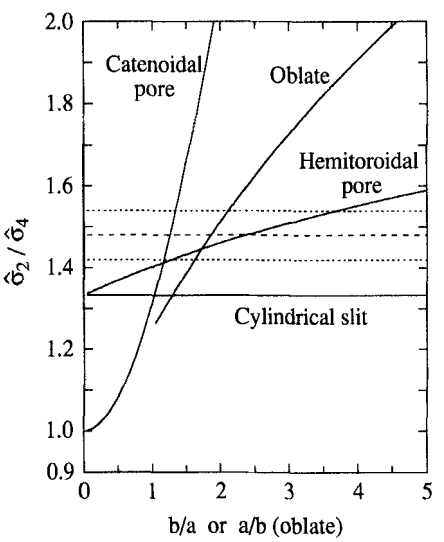

Figure 2. Ratio of geometrical parameters for various bilayer defect models (cf. text). The dotted lines represent the experimental result (with propagated errors), derived from the data in figure 1 (*b*).

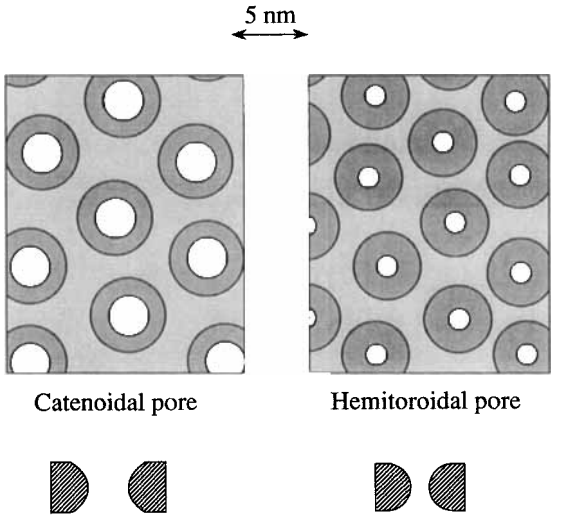

Figure 3. Top and side projections of bilayer with pore defects, as deduced from the corresponding b/a values in figure 2. The absolute length scale is based on the X-ray repeat distance.

for orientational disorder of the aggregates and if we calculate the spectral densities $J^{ms}_{nn}(k\omega_0)$ exactly [133], without invoking the lorentzian approximation equation (4.6).)

We are thus left with the two pore models. The values of λ and P, obtained from σ_2 and σ_4, allow us (assuming a laterally uniform counterion distribution) to construct the projected views in figure 3 of the perforated bilayer. Although a large fraction of the total interface is curved (76 per cent and 48 per cent, respectively, for hemitoroidal and catenoidal pores), only a small fraction of the bilayer plane is permeable to water and ions (6 per cent and 12 per cent, respectively). The catenoidal pore is a minimal surface [154] with zero mean curvature, while the hemitoroidal pore has a positive average mean curvature, as in the adjacent nematic and hexagonal phases. (A more general ribbon model, with elliptic edges, is also consistent with the data, and appears to be energetically more favourable than the pore geometries [71].)

The structures shown in figure 3 are based entirely on the geometrical parameters σ_2 and σ_4 and, hence, do not involve absolute dimensions. To obtain the length scales of the structures, we can either invoke the correlation times τ_n (cf. § 4.4) or determine the lamellar repeat distance by X-ray diffraction. In the present case the two approaches give similar, and reasonable, results: a bilayer thickness of *c.* 3 nm and an inner pore radius of *c.* 1 nm [71].

7.2. *2D mesophases*

Lyotropic phases whose microstructural elements are of indefinite length in one dimension and are periodically ordered in the other two dimensions are sometimes called canonic mesophases [23]. This class of liquid crystals includes the normal and reversed hexagonal phases of plane group p6mm and the rectangular phases, with the most common plane groups c2mm and p2gg.

In the ground state microstructure of canonic mesophases (disregarding collective fluctuations), the local interface normal is everywhere perpendicular to the highest symmetry axis of the liquid crystal ($\theta_{CN}=\pi/2$). This fact greatly simplifies the spin

relaxation behaviour, reducing the number of ICFSDs $J^{ms}_{\lambda}(k\omega_0)$ associated with the microstructure (cf. table 2) to one for hexagonal phases, two for rectangular, and three for oblique mesophases [124].

The aggregate shape in canonic mesophases is usually represented by a circular or elliptic cylinder [32] (or by a ribbon with a semi-circle capped rectangular cross-section [30]). In a hexagonal phase, where the cylindrical aggregates may be locally elliptic [19, 22], the six non-adiabatic ICFSDs are, under the assumptions of equations (4.2)–(4.4), given by

$$J^{C}_{nn}(k\omega_0) = J^{loc}(0) + \delta_{n2} J^{ms}_{22}(k\omega_0), \tag{7.7}$$

where $J^{ms}_{22}(\omega)$ is the cosine transform of the TCF

$$G^{ms}_{22}(\tau) = \tfrac{3}{8}\bar{V}^2_S[S^2_C g_D(\tau) + (1 - S^2_C) g_D(\tau) g_C(\tau)]. \tag{7.8}$$

Here $S_C = \langle \cos(2\phi_C) \rangle$ is the order parameter characterizing the cross-sectional shape. For an elliptic cylinder of aspect ratio ρ (and eccentricity, $\varepsilon = (1 - \rho^{-2})^{1/2}$), S_C can be expressed in terms of complete elliptic integrals as [32]

$$S_C = \frac{2}{\rho^2 - 1}\left[\frac{K(\varepsilon^2)}{E(\varepsilon^2)} - 1\right] - 1. \tag{7.9}$$

Equation (7.8) contains two reduced TCFs: $g_C(\tau)$ is associated with surface diffusion on the biaxial cylinder, modulating the orientation ϕ_C of the local interface normal with respect to the aggregate, and $g_D(\tau)$ is associated with diffusion of the spin-bearing species between differently oriented cross-sections or reorientation of the (local) aggregate cross-section, modulating the angle ϕ_D describing the orientation of the cross-section, with respect to the liquid crystal. These reduced TCFs are simply

$$g_D(\tau) = \langle \cos[2(\phi_D - \phi^0_D)] \rangle, \tag{7.10}$$

$$g_C(\tau) = (1 - S^2_C)^{-1}[\langle \cos[2(\phi_C - \phi^0_C)] \rangle - S^2_C]. \tag{7.11}$$

In the limit of a circular cross-section, $S_C = 0$ and equation (7.8) reduces (after Fourier transformation) to equation (5.18). (In this case we can set $g_D(\tau) = g_D(0) = 1$, since the rotational diffusion of the cylinder around its axis is much slower than surface diffusion.)

We now consider the ^{23}Na relaxation data obtained from the counterions in a homeotropically aligned sample of the hexagonal phase in the system sodium dodecyl sulphate/water/decanol [69, 70]. Figure 4 (*a*) shows the orientation dependence of the non-adiabatic LFSDs [70], yielding, by way of equation (3.5), the six non-adiabatic ICFSDs shown in figure 4 (*b*). According to equation (7.7), four of these should be equal, reflecting only the local dynamics. The slight deviation from this idealized picture can be accounted for by the flexibility of the cylindrical aggregates (closely related to the bend elastic modulus of the hexagonal phase [149]). The long wavelength fluctuations associated with this flexibility are clearly manifest in the adiabatic ICFSDs [70].

Assuming that the aggregates are circular cylinders, the two ICFSDs $J^{C}_{11}(\omega_0)$ and $J^{C}_{22}(2\omega_0)$ can be used to determine the residual quadrupole coupling constant and the correlation time τ_S in equation (5.18). With the cylinder radius obtained from X-ray diffraction data, the surface diffusion coefficient D_S of the Na^+ counterions can thus be deduced. In this case we obtained [69, 70] $D_S = (4{\cdot}4 \pm 0{\cdot}4) \times 10^{-10}\,m^2\,s^{-1}$ at 25°C, which is only a factor of three smaller than for an infinitely dilute bulk electrolyte solution. From the ^{2}H relaxation of the α-deuteriated dodecyl sulphate surfactant in the same mesophase [69], we determined in a similar way the lateral diffusion

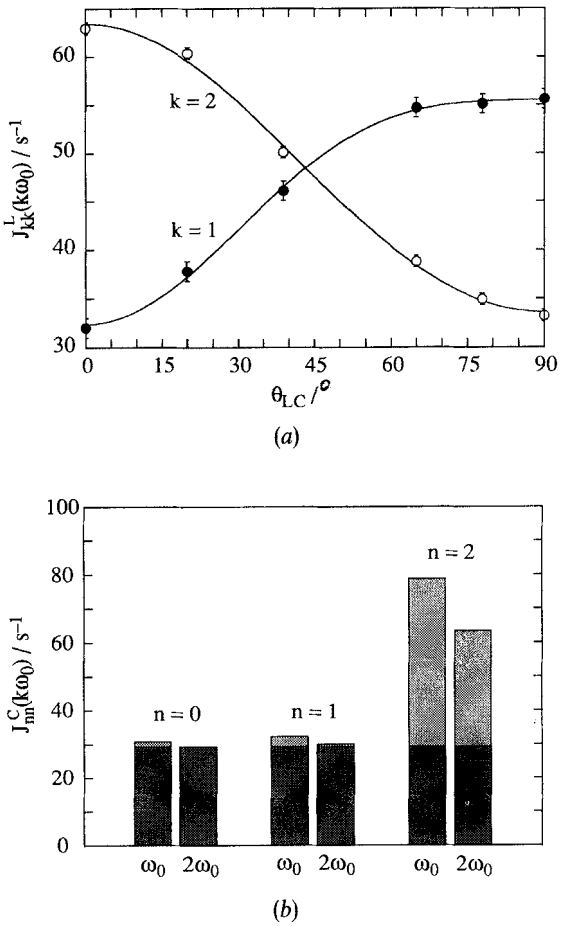

Figure 4. ^{23}Na relaxation data from counterions in the hexagonal phase of the system sodium dodecyl sulphate/water/decanol [70]. (*a*) Variation of the non-adiabatic lab-frame spectral densities with the crystal orientation, θ_{LC}. (*b*) Crystal-frame spectral densities derived, according to equation (3.5), from the fits in (*a*). The dark area represents the local motion contribution $J^{loc}(0)$.

coefficient of the surfactant: $D_S = (1{\cdot}4 \pm 0{\cdot}2) \times 10^{-10}\,m^2\,s^{-1}$, i.e. only a factor of three smaller than for the counterion.

In reversed hexagonal phases the radius of the aqueous cylinders can be varied in a controlled way, allowing a direct verification of the a^2 dependence of the correlation time. This was done in a ^{23}Na relaxation study of the reversed hexagonal phase in the system Aerosol OT/water/iso-octane, yielding $D_S = (2{\cdot}8 \pm 0{\cdot}3) \times 10^{-10}\,m^2\,s^{-1}$ at 20·6°C (a factor of 3·6 less than the limiting bulk value) [68].

As in a lamellar phase, normal diffusion (perpendicular to the cylindrical interface) also contributes to the ICFSDs in a hexagonal phase. Since normal and lateral diffusion cannot be separated in cylindrical symmetry, both $J^C_{00}(\omega)$ and $J^C_{22}(\omega)$ are affected. To assess the validity of the surface diffusion approximation, equation (5.18), the contributions to these spectral densities from counterion diffusion in the 3D space

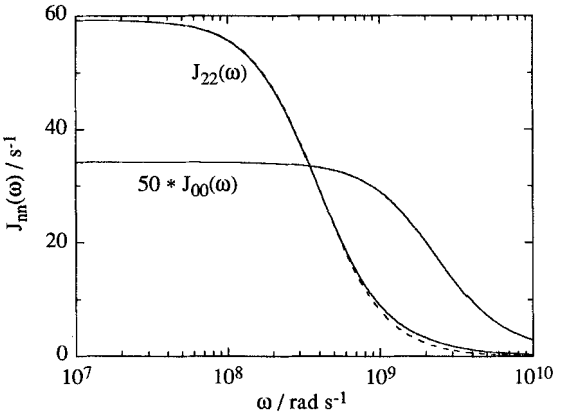

Figure 5. Crystal-frame spectral density contributions from counterion diffusion in the 3D space outside the cylindrical aggregates in a hexagonal phase [69]. The dashed lorentzian dispersion curve corresponds to the surface diffusion approximation, equation (5.18).

outside the cylinders can be calculated numerically [138], taking into account the electrostatic interactions (in a mean-field approximation) among the counterions and with the oppositely charged cylinder. The result of such a calculation, for the hexagonal phase discussed above [69], is shown in figure 5. The normal diffusion contribution to $J^C_{00}(\omega)$ is seen to be negligible, while $J^C_{22}(\omega)$ remains very nearly lorentzian. Moreover, the effective correlation time characterizing this lorentzian dispersion does not differ significantly from τ_S in equation (5.18).

7.3. *3D mesophases*

Among the lyotropic mesophases that are periodic in three dimensions, those of cubic symmetry are by far the most widely occurring [10, 40, 157], although several 3D mesophases of lower symmetry are known [11, 155, 156]. According to the topology of their microstructure, cubic phases are either of the micellar type, containing closed (usually small) surfactant aggregates, or of the bicontinuous type, with both polar and non-polar regions connected over macroscopic distances in three dimensions. Several spin relaxation studies have been reported on cubic phases of both types [42, 48, 62–67]. Micellar cubic phases are usually modelled in terms of spheroidal aggregates [127, 128]. The analysis of spin relaxation data from such phases involves diffusion on the spheroidal aggregate surfaces, restricted rotational diffusion of the aggregates, and slower exchange processes [123, 133]. In the following we focus on bicontinuous cubic phases.

The microstructure of bicontinuous cubic mesophases is usually modelled in terms of a class of minimal surfaces that are periodic in three dimensions and free from self-intersections [158–162]. (A minimal surface may be defined as a surface whose mean curvature vanishes at every point [154, 163].) These triply periodic minimal surfaces (TPMS) are then taken to define the bisecting surfaces of the polar (aqueous) or non-polar (bilayer) regions in normal and reversed cubic phases, respectively. One example of a cubic TPMS, the so-called gyroid surface [164], is shown in figure 6.

In a cubic phase there are two ICFSDs (cf. table 2), associated with the irreducible representations E and T_2 of the octahedral point group [123]. In general these ICFSDs

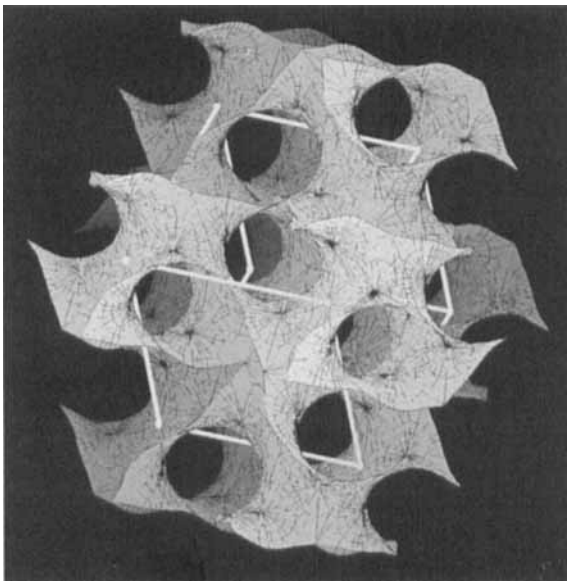

Figure 6. The gyroid minimal surface, with the cubic unit cell inscribed ($\chi_E = -8$).

may contain contributions from all three terms in equation (4.1). Whereas long wavelength fluctuations [165] do not seem to contribute significantly [48], surface diffusion has been implicated as a major source of spin relaxation in bicontinuous cubic liquid crystals [42, 62, 67].

The TCFs describing diffusion over a cubic TPMS can be numerically computed along the lines described in § 5. Due to the high symmetry of these surfaces, however, it is reasonable to assume that the TCFs decay exponentially (as for surface diffusion on a sphere, cf. equation (5.17)) and to define the correlation times (with $\lambda = \mathrm{E}$ or T_2) as

$$\tau_S^\lambda = -G_\lambda^{sd}(0)/\dot{G}_\lambda^{sd}(0), \tag{7.12}$$

where the dot signifies a time derivative. This definition ensures that the exponential TCF approximation is exact to linear order in time [166]. By exploiting the fact that a minimal surface can be conformally mapped on to the unit sphere [154, 163], it can be shown that the initial slope of both TCFs is given exactly by [134]

$$\dot{G}_\lambda^{sd}(0) = \tfrac{6}{5} D_S \langle K \rangle, \tag{7.13}$$

where D_S is the surface diffusion coefficient and $\langle K \rangle$ is the average gaussian curvature of the TPMS. The latter quantity is related to the surface area A_S (per cubic unit cell) and the topology (Euler characteristic, χ_E) of the TPMS through the Gauss–Bonnet theorem [154],

$$\langle K \rangle = \frac{2\pi\chi_E}{A_S}. \tag{7.14}$$

Finally, the initial TCFs $G_\lambda^{sd}(0)$, which are the fluctuation amplitudes A_λ in equation (4.6), can be related to a single geometrical parameter, conveniently chosen as the cubic order parameter $Q = \langle P_4(\cos\theta_{CN}) \rangle$ [123].

Spin relaxation studies of macroscopically oriented (single crystal) cubic phases have not yet been reported. For powder samples, it is the isotropically averaged TCF that is probed. Within the short time approximation in equation (7.12), the effective correlation time becomes [134]

$$\tau_S = -\frac{1}{6D_S\langle K\rangle}. \tag{7.15}$$

In table 3 we give the correlation time τ_S, calculated from equations (7.14) and (7.15) and the known surface area and Euler characteristic [167], for several cubic TPMS, among them Schwarz's D and P surfaces, the gyroid surface G, and the Neovius surface C(P). It is seen that the correlation time τ_S for surface diffusion on a cubic TPMS is always considerably shorter than the correlation time for surface diffusion on a sphere inscribed in the cubic unit cell. The monotonic decrease of τ_S down the table is not due to the variation of the surface area (A_S increases monotonically down the table), but rather to the increasing topological complexity of the surfaces ($-\chi_E$ increases monotonically down the table). A particularly valuable feature of the spin relaxation method is its ability to discriminate (*via* τ_S) among different microstructures that belong to the same space group, such as the P and C(P) surfaces, and therefore yield the same X-ray diffraction indices. Finally, we note that the exact result in equation (7.13) remains valid for non-cubic TPMS, for example, the tetragonally and rhombohedrally distorted D and P surfaces [168], which have been used to model the microstructure in non-cubic 3D mesophases [33, 34].

7.4. *Nematic phases*

Three types of nematic phase occur in lyotropic systems [9, 13, 169–174]: the calamitic (N_C) and discotic (N_D) uniaxial phases and the biaxial phase (N_B). All lyotropic nematic phases are believed to consist of closed surfactant aggregates (micelles), which are necessarily of biaxial shape in the N_D phase. The aggregate shape in the uniaxial phases is often described in terms of prolate (N_C) or oblate (N_D) spheroids, although some authors argue that the aggregates are biaxial in all three nematic phases [126, 174]. Although traditionally regarded as members of the liquid crystal family, the nematic phases are perhaps more aptly referred to as anisotropic fluids, since they lack long range translational order.

In spin relaxation studies of nematic phases, we encounter two major difficulties. First, the fast magnetic alignment of nematic fluids precludes relaxation anisotropy measurements with conventional methods (cf. § 3.1). Even if the alignment problem can

Table 3. Effective correlation time, τ_S, for diffusion on cubic minimal surfaces.

Surface	Space group	τ_S†
D	$Pn\bar{3}m$	0·6108
P	$Im\bar{3}m$	0·3732
G	$Ia\bar{3}d$	0·2460
I-WP	$Im\bar{3}m$	0·1839
C(P)	$Im\bar{3}m$	0·1397
F-RD	$Fm\bar{3}m$	0·0754

†In units of the correlation time, $a^2/(24D_S)$, for surface diffusion on a sphere of diameter equal to the cubic lattice parameter a.

be overcome, the very large adiabatic spectral density $J^{C}_{11}(0)$, due to long wavelength fluctuations (cf. § 6.3), will probably restrict the useful relaxation experiments to those involving the non-adiabatic central line of nuclei with half-integral spin. For these reasons, relaxation dispersion measurements may come to play an important role in the study of nematic phases.

The second difficulty in spin relaxation studies of nematic phases is related to their microstructure. To specify the microstructure (as defined in § 1) of a nematic phase, we need to determine the size and shape of the aggregates as well as their orientational order. This specification requires between two and four parameters, depending on the symmetry of the phase and of the aggregates. The dynamic description requires still more parameters.

For simplicity, we consider here only uniaxial nematic phases composed of spheroidal aggregates. Two processes contribute to the spectral densities $J^{ms}_{nn}(k\omega_0)$: surface diffusion and restricted aggregate reorientation. The corresponding TCFs are of the form [133]

$$G^{ms}_{nn}(\tau) = \bar{V}_S^2 S^2_{shp}\, g^{rot}_{n0}(\tau) + \bar{V}_S^2 \sum_{p=0}^{2} (2-\delta_{p0})[g^{rot}_{np}(\tau) + \delta_{n0}\delta_{p0} S^2_{nem}] g^{sd}_{pp}(\tau). \tag{7.16}$$

The first term describes the restricted tumbling of the spheroidal micelle, while the three terms in the sum describe the combined effect of micelle rotation and surface diffusion. $S_{nem} = \langle P_2(\cos\theta_{DA})\rangle$ is the usual nematic order parameter [25], with θ_{DA} the angle between the aggregate axis and the phase director. The order parameter $S_{shp} = \langle P_2(\cos\theta_{AN})\rangle$ with θ_{AN} the angle between the local interface normal and the aggregate axis, is a purely geometrical quantity, characterizing the aggregate shape (assuming a uniform surface distribution of the spin-bearing species). For spheroids of axial ratio ρ [133, 175]

$$S_{shp} = -\frac{2+\rho^2+(\rho^2-4)F_{pr}}{2(\rho^2-1)(1+F_{pr})} \qquad \text{(prolate)}, \tag{7.17a}$$

$$S_{shp} = \frac{2\rho^2+1+(1-4\rho^2)F_{ob}}{2(\rho^2-1)(1+F_{ob})} \qquad \text{(oblate)}, \tag{7.17b}$$

$$F_{pr} = \frac{\rho^2 \arccos(1/\rho)}{(\rho^2-1)^{1/2}}, \tag{7.18a}$$

$$F_{ob} = \frac{\operatorname{arccosh}(\rho)}{\rho(\rho^2-1)^{1/2}}. \tag{7.18b}$$

The reduced TCFs $g^{sd}_{pp}(\tau)$ for diffusion on a spheroidal surface can be calculated by the methods described in § 5 [133]. The reduced TCFs $g^{rot}_{np}(\tau)$ for restricted micelle reorientation are more difficult to treat rigorously, since reorientation in a nematic phase is a highly cooperative process. As long as we restrict our attention to the six non-adiabatic ICFSDs, however, it seems reasonable to model this process as rotational diffusion of individual micelles subject to an even uniaxial mean torque, determined self-consistently by the nematic order parameter S_{nem} [72, 73, 129–132].

If micelle reorientation is slow compared to surface diffusion and compared to the Larmor frequency ω_0, which is typically the case [72], the non-adiabatic ICFSDs are unaffected by the reorientational dynamics, and

$$J^{C}_{nn}(k\omega_0) = J^{loc}(0) + \bar{V}_S^2 \sum_{p=0}^{2} (2-\delta_{p0})[g^{rot}_{np}(0) + \delta_{n0}\delta_{p0} S^2_{nem}] J^{sd}_{pp}(k\omega_0). \tag{7.19}$$

The quantities enclosed by brackets can be expressed, in a model-independent way, as linear combinations of the two nematic order parameters S_{nem} and $Q_{nem} = \langle P_4(\cos\theta_{DA})\rangle$ [133]. By introducing a plausible one parameter functional form for the potential of mean torque, Q_{nem} can be eliminated as an independent parameter [72, 176]. The six non-adiabatic ICFSDs are then determined by five parameters: the local motion contribution $J^{loc}(0)$, the residual quadrupole coupling constant $\bar{\chi}$ (proportional to $\bar{V}_S$), the nematic order parameter S_{nem}, the micellar axial ratio ρ, and the characteristic time a^2/D_S for surface diffusion (a is one of the semi-axes of the spheroid). One of the parameters $\bar{\chi}$, S_{nem}, and ρ can be eliminated by invoking the quadrupole splitting, which is proportional to $\bar{\chi}S_{shp}S_{nem}$ [72]. The problem is, of course, that the individual ICFSDs are not usually available, since nematic phases do not lend themselves to conventional relaxation anisotropy measurements. There are then only the two non-adiabatic LFSDs and the quadrupole splitting, which obviously do not suffice to determine five parameters. There are two possible solutions to this dilemma: to measure the relaxation dispersion or to determine two of the parameters in an orientable mesophase with similar local properties [72].

The N_C and N_D phases in the system sodium dodecyl sulphate/water/decanol [177] have been investigated by spin relaxation (at a single magnetic field) of ^2H in the α-deuteriated surfactant and of ^{23}Na in the counterion [72, 73]. In these studies we determined the micelle size (ρ) and order (S_{nem}), as well as the viscoelastic properties of the phases, over the temperature range where these phases are stable. The axial ratio ρ of the micelles was found to be in the range 3–4 in both phases, with no significant temperature dependence. The nematic order parameter S_{nem} decreases with temperature as expected, but near the nematic–isotropic transition the temperature dependence is much stronger than predicted by the conventional (Maier–Saupe) mean field theory [178, 179]. This is shown in figure 7.

In contrast to thermotropic nematics [180], long wavelength fluctuations do not seem to contribute significantly to the non-adiabatic spectral densities in lyotropic nematics [72, 73]. The adiabatic LFSD $J^L_{00}(0)$, on the other hand, is dominated by the effects of long wavelength fluctuations and can thus be used to study the viscoelastic

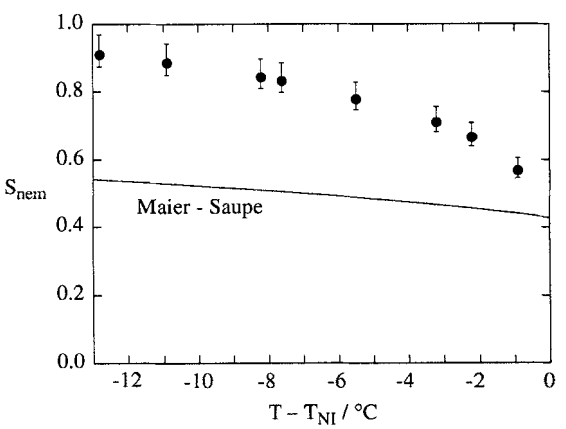

Figure 7. Temperature dependence of the nematic order parameter, S_{nem}, in the N_C phase of the system sodium dodecyl sulphate/water/decanol, derived from non-adiabatic ^{23}Na relaxation data [72]. The curve is the prediction of the Maier–Saupe theory.

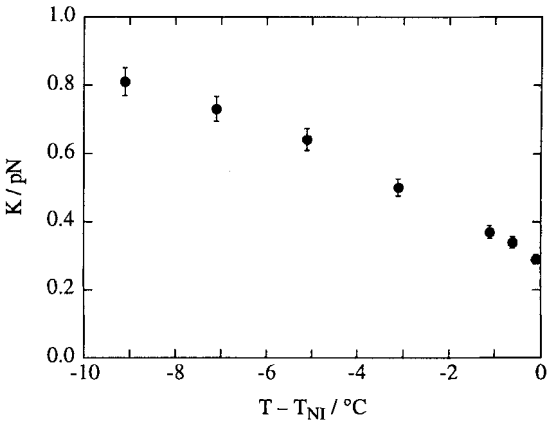

Figure 8. Temperature dependence of the effective elastic modulus, K, in the N_C phase of the system sodium dodecyl sulphate/water/decanol, derived from adiabatic ^{23}Na relaxation data [73].

properties of the nematic fluid. As an example, figure 8 shows the temperature dependence of the effective elastic modulus K in the N_C phase of the aforementioned system [73], determined from ^{23}Na relaxation data and equation (6.10 *a*).

Our work on spin relaxation in lyotropic liquid crystals has been supported by the Swedish Natural Science Research Council (NFR).

References

[1] SKOULIOS, A., 1967, *Adv. Colloid Interf. Sci.*, **1**, 79.
[2] LUZZATI, V., 1968, *Biological Membranes*, Vol. 1, edited by D. Chapman (Academic Press), p. 71.
[3] WINSOR, P. A., 1968, *Chem. Rev.*, **68**, 1.
[4] LUZZATI, V., and TARDIEU, A., 1974, *A. Rev. phys. Chem.*, **25**, 79.
[5] FONTELL, K., 1974, *Liquid Crystals and Plastic Crystals*, Vol. 2, edited by G. W. Gray and P. A. Winsor (Ellis Horwood), p. 80.
[6] EKWALL, P., 1975, *Advances in Liquid Crystals*, Vol. 1, edited by G. H. Brown (Academic Press), p. 1.
[7] CHARVOLIN, J., and TARDIEU, A., 1978, *Solid State Physics*, Vol. 14, edited by F. Seitz and D. Turnbull (Academic Press), p. 209.
[8] TIDDY, G. J. T., 1980, *Phys. Rep.*, **57**, 1.
[9] FORREST, B. J., and REEVES, L. W., 1981, *Chem. Rev.*, **81**, 1.
[10] FONTELL, K., 1990, *Colloid Polym. Sci.*, **268**, 264.
[11] KÉKICHEFF, P., and CABANE, B., 1987, *J. Phys., Paris*, **48**, 1571.
[12] HUSSON, F., MUSTACCHI, H., and LUZZATI, V., 1960, *Acta crystallogr.*, **13**, 668.
[13] YU, L. J., and SAUPE, A., 1980, *Phys. Rev. Lett.*, **45**, 1000.
[14] STRÖM, P., and ANDERSON, D. M., 1992, *Langmuir*, **8**, 691.
[15] HOLMES, M. C., and CHARVOLIN, J., 1984, *J. phys. Chem.*, **88**, 810.
[16] KÉKICHEFF, P., CABANE, B., and RAWISO, M., 1984, *J. Phys. Lett., Paris*, **45**, 813.
[17] ALLAIN, M., and KLÉMAN, M., 1987, *J. Phys. Paris*, **48**, 1799.
[18] HENDRIKX, Y., CHARVOLIN, J., KÉKICHEFF, P., and ROTH, M., 1987, *Liq. Crystals*, **2**, 677.
[19] HENDRIKX, Y., and CHARVOLIN, J., 1988, *Liq. Crystals*, **3**, 265.
[20] HOLMES, M. C., CHARVOLIN, J., and REYNOLDS, D. J., 1988, *Liq. Crystals*, **3**, 1147.
[21] RANÇON, Y., and CHARVOLIN, J., 1988, *J. phys. Chem.*, **92**, 6339.
[22] HENDRIKX, Y., and CHARVOLIN, J., 1992, *Liq. Crystals*, **11**, 677.

[23] HELFRICH, W., 1981, *Physics of Defects*, edited by R. Balian, M. Kléman, and J. P. Poirer (North-Holland), p. 714.
[24] BAGDASSARIAN, C. K., ROUX, D., BEN-SHAUL, A., and GELBART, W. M., 1991, *J. chem. Phys.*, **94,** 3030.
[25] DE GENNES, P. G., 1974, *The Physics of Liquid Crystals* (Clarendon Press).
[26] SEELIG, J., 1977, *Q. Rev. Biophys.*, **10,** 353.
[27] CHARVOLIN, J., and HENDRIKX, Y., 1985, *Nuclear Magnetic Resonance of Liquid Crystals*, edited by J. W. Emsley (D. Reidel), p. 449.
[28] BODEN, N., and JONES, S. A., 1985, *Nuclear Magnetic Resonance of Liquid Crystals*, edited by J. W. Emsley (D. Reidel), p. 473.
[29] HALLE, B., and WENNERSTRÖM, H., 1981, *J. chem. Phys.*, **75,** 1928.
[30] DOANE, J. W., 1985, *Nuclear Magnetic Resonance of Liquid Crystals*, edited by J. W. Emsley (D. Reidel), p. 413.
[31] GOLDFARB, D., POUPKO, R., LUZ, Z., and ZIMMERMAN, H., 1983, *J. chem. Phys.*, **79,** 4035.
[32] QUIST, P.-O., and HALLE, B., 1988, *Molec. Phys.*, **65,** 547.
[33] HENRIKSSON, U., BLACKMORE, E. S., TIDDY, G. J. T., and SÖDERMAN, O., 1992, *J. phys. Chem.*, **96,** 3894.
[34] ANDERSON, D. M., 1990, *J. Phys. Colloque, Paris*, **C7,** 1.
[35] CALLAGHAN, P. T., 1984, *Aust. J. Phys.*, **37,** 359.
[36] STILBS, P., 1987, *Progr. NMR Spectrosc.*, **19,** 1.
[37] KÄRGER, J., PFEIFER, H., and HEINK, W., 1988, *Adv. magn. Reson.*, **12,** 1.
[38] TIDDY, G. J. T., 1977, *J. chem. Soc. Faraday Trans.*, **73,** 1731.
[39] KUO, A.-L., and WADE, C. G., 1979, *Biochemistry*, **18,** 2300.
[40] LINDBLOM, G., and RILFORS, L., 1989, *Biochem. biophys. Acta*, **998,** 221.
[41] UKLEJA, P., CHIDICHIMO, G., and PHOTINOS, P., 1991, *Liq. Crystals*, **9,** 359.
[42] CHARVOLIN, J., and RIGNY, P., 1973, *J. chem. Phys.*, **58,** 3999.
[43] DAVIS, J. H., JEFFREY, K. R., and BLOOM, M., 1978, *J. magn. Reson.*, **29,** 191.
[44] WONG, T. C., and JEFFREY, K. R., 1982, *Molec. Phys.*, **46,** 1.
[45] JEFFREY, K. R., WONG, T. C., and TULLOCH, A. P., 1984, *Molec. Phys.*, **52,** 307.
[46] CHACHATY, C., and QUAEGEBEUR, J. P., 1984, *Molec. Phys.*, **52,** 1081.
[47] BOZONNET-FRENOT, M. P., MARCHAL, J. P., and CANET, D., 1987, *J. phys. Chem.*, **91,** 89.
[48] KÜHNER, W., ROMMEL, E., NOACK, F., and MEIER, P., 1987, *Z. Naturf.* (*a*), **42,** 127.
[49] CHACHATY, C., and KORB, J.-P., 1988, *J. phys. Chem.*, **92,** 2834.
[50] CHACHATY, C., CANIPAROLI, J.-Ph., FAURE, A., and TISTCHENKO, A. M., 1988, *J. phys. Chem.*, **92,** 6330.
[51] CHACHATY, C., and BREDEL, T., 1991, *J. phys. Chem.*, **95,** 5335.
[52] BROWN, M. F., SEELIG, J., and HÄBERLEN, U., 1979, *J. chem. Phys.*, **70,** 5045.
[53] GRIFFIN, R. G., 1981, *Meth. Enzymol.*, **72,** 108.
[54] POPE, J. M., WALKER, L., CORNELL, B. A., and SEPAROVIC, F., 1982, *Molec. Crystals liq. Crystals*, **89,** 137.
[55] DAVIS, J. H., 1983, *Biochem. biophys. Acta*, **737,** 117.
[56] FUSON, M. M., and PRESTEGARD, J. H., 1983, *J. Am. chem. Soc.*, **105,** 168.
[57] BLOOM, M., and SMITH, I. C. P., 1985, *Progress in Protein-Lipid Interactions*, Vol. 1, edited by A. Watts and J. J. H. H. M. De Pont (Elsevier), p. 1.
[58] JARRELL, H. C., SMITH, I. C. P., JOVALL, P. A., MANTSCH, H. H., and SIMINOVITCH, D. J., 1988, *J. chem. Phys.*, **88,** 1260.
[59] SIMINOVITCH, D. J., RUOCCO, M. J., OLEJNICZAK, E. T., DAS GUPTA, S. K., and GRIFFIN, R. G., 1988, *Biophys. J.*, **54,** 373.
[60] ROMMEL, E., NOACK, F., MEIER, P., and KOTHE, G., 1988, *J. phys. Chem.*, **92,** 2981.
[61] MAYER, C., GRÖBNER, G., MÜLLER, K., WEISZ, K., and KOTHE, G., 1990, *Chem. Phys. Lett.*, **165,** 155.
[62] ERIKSSON, P.-O., KHAN, A., and LINDBLOM, G., 1982, *J. Phys. Chem.*, **86,** 387.
[63] ERIKSSON, P.-O., LINDBLOM, G., and ARVIDSSON, G., 1985, *J. phys. Chem.*, **89,** 1050.
[64] SÖDERMAN, O., WALDERHAUG, H., HENRIKSSON, U., and STILBS, P., 1985, *J. phys. Chem.*, **89,** 3693.
[65] SÖDERMAN, O., and HENRIKSSON, U., 1987, *J. chem. Soc. Faraday Trans. 1*, **83,** 1515.
[66] ERIKSSON, P.-O., LINDBLOM, G., and ARVIDSSON, G., 1987, *J. phys. Chem.*, **91,** 846.
[67] SÖDERMAN, O., OLSSON, U., and WONG, T. C., 1989, *J. phys. Chem.*, **93,** 7474.
[68] FURÓ, I., HALLE, B., QUIST, P.-O., and WONG, T. C., 1990, *J. phys. Chem.*, **94,** 2600.

[69] QUIST, P.-O., HALLE, B., and FURÓ, I., 1991, *J. chem. Phys.*, **95,** 6945.
[70] QUIST, P.-O., BLOM, I., and HALLE, B., 1992, *J. magn. Reson.*, **100,** 267.
[71] QUIST, P.-O., and HALLE, B., *Phys. Rev.* A (submitted).
[72] QUIST, P.-O., HALLE, B., and FURÓ, I., 1992, *J. chem. Phys.*, **96,** 3875.
[73] HALLE, B., QUIST, P.-O., and FURÓ, I., 1992, *Phys. Rev.* A, **45,** 3763.
[74] SPIESS, H. W., 1985, *Adv. Polym. Sci.*, **66,** 23.
[75] VOLD, R. L., and VOLD, R. R., 1983, *Isr. J. Chem.*, **23,** 315.
[76] VOLD, R. R., 1985, *Nuclear Magnetic Resonance of Liquid Crystals*, edited by J. W. Emsley (D. Reidel), p. 253.
[77] FURÓ, I., HALLE, B., and WONG, T. C., 1988, *J. chem. Phys.*, **89,** 5382.
[78] FURÓ, I., and HALLE, B., 1989, *J. chem. Phys.*, **91,** 42.
[79] FURÓ, I., and HALLE, B., 1992, *J. magn. Reson.*, **98,** 388.
[80] FURÓ, I., and HALLE, B., 1992, *Molec. Phys.*, **76,** 1169, and references therein.
[81] FURÓ, I., 1992, *Chem. Phys. Lett.*, **194,** 435.
[82] ABRAGAM, A., 1961, *The Principles of Nuclear Magnetism* (Clarendon Press).
[83] BLUM, K., 1981, *Density Matrix Theory and Applications* (Plenum Press).
[84] SANCTUARY, B. C., and HALSTEAD, T. K., 1990, *Adv. magn. opt. Reson.*, **15,** 79.
[85] SZYMANSKI, S., GRYFF-KELLER, A. M., and BINSCH, G., 1986, *J. magn. Reson.*, **68,** 399.
[86] WERBELOW, L., and POUZARD, G., 1981, *J. phys. Chem.*, **85,** 3887.
[87] JACOBSEN, J. P., BILDSØE, H. K., and SCHAUMBURG, K., 1976, *J. magn. Reson.*, **23,** 153.
[88] DAVIS, J. H., JEFFREY, K. R., BLOOM, M., VALIC, M. I., and HIGGS, T. P., 1976, *Chem. Phys. Lett.*, **42,** 390.
[89] VOLD, R. L., and VOLD, R. R., 1981, *J. magn. Reson.*, **42,** 173.
[90] GRUWEL, M. L. H., 1991, *J. phys. Chem.*, **95,** 10109, and references therein.
[91] VOLD, R. R., and VOLD, R. L., 1977, *J. chem. Phys.*, **66,** 4018.
[92] DOLINSEK, J., 1991, *J. magn. Reson.*, **92,** 312.
[93] AHMAD, S. B., PACKER, K. J., and RAMSDEN, J. M., 1977, *Molec. Phys.*, **33,** 857.
[94] BLOOM, M., and STERNIN, E., 1987, *Biochemistry*, **26,** 2101.
[95] VEGA, A. J., POUPKO, R., and LUZ, Z., 1989, *J. magn. Reson.*, **83,** 111.
[96] MÜLLER, K., POUPKO, R., and LUZ, Z., 1990, *J. magn. Reson.*, **90,** 19.
[97] STOHRER, J., GRÖBER, G., REIMER, D., WEISZ, K., MAYER, C., and KOTHE, G., 1991, *J. chem. Phys.*, **95,** 672.
[98] NOACK, F., 1986, *Progr. NMR Spectrosc.*, **18,** 171.
[99] NOACK, F., 1992, *The Molecular Dynamics of Liquid Crystals*, edited by G. R. Luckhurst (Kluwer Academic) (in the press).
[100] SCHWEIKERT, K. H., and NOACK, F., 1992, *Molec. Crystals liq. Crystals*, **212,** 33.
[101] WERBELOW, L., 1979, *J. chem. Phys.*, **70,** 5381.
[102] BRINKMANN, D., MALI, M., ROOS, J., MESSER, R., and BIRLI, H., 1982, *Phys. Rev.* B, **26,** 4810.
[103] ELIAV, U., and NAVON, G., 1991, *J. chem. Phys.*, **95,** 7114.
[104] CORTIEU, J., ALDERMAN, D. W., GRANT, D. M., and BAYLES, J. P., 1982, *J. chem. Phys.*, **77,** 723.
[105] PHOTINOS, D. J., BOS, P. J., DOANE, J. W., and NEUBERT, M., E., 1979, *Phys. Rev.* A, **20,** 2203.
[106] DIEHL, P., and KHETRAPAL, C. L., 1967, *Molec. Phys.*, **14,** 283.
[107] EMSLEY, J. W., LINDON, J. C., LUCKHURST, G. R., and SHAW, D., 1973, *Chem. Phys. Lett.*, **19,** 345.
[108] CARR, E. F., 1963, *J. chem. Phys.*, **39,** 1979.
[109] HELFRICH, W., 1969, *J. chem. Phys.*, **51,** 4092.
[110] BOS, P. J., PIRS, J., UKLEJA, P., DOANE, J. W., and NEUBERT, M. E., 1977, *Molec. Crystals liq. Crystals*, **40,** 59. TARR, C. E., VOSMAN, F., and WHALLEY, L. R., 1977, *J. chem. Phys.*, **67,** 868.
[111] HOLMES, M. C., REYNOLDS, D. J., and BODEN, N., 1987, *J. phys. Chem.*, **91,** 5257.
[112] OLIVEIRA, E. A., LIÉBERT, L., and FIGUEIREDO NETO, A. M., 1989, *Liq. Crystals*, **5,** 1669.
[113] HENDRIKX, Y., CHARVOLIN, J., RAWISO, M., LIÉBERT, L., and HOLMES, M. C., 1983, *J. phys. Chem.*, **87,** 3991.
[114] LÜHMANN, B., FINKELMANN, H., and REHAGE, G., 1985, *Makromolek. Chem.*, **186,** 1059.
[115] CHACHATY, C., and QUAEGEBEUR, J. P., 1983, *J. phys. Chem.*, **87,** 4341.
[116] GUTMAN, H., LUZ, Z., WACHTEL, E. J., POUPKO, R., and CHARVOLIN, J., 1990, *Liq. Crystals*, **7,** 335.

[117] De Vries, J. J., and Berendsen, H. J. C., 1969, *Nature, Lond.*, **221,** 1139.
[118] Jarrell, H. C., Jovall, P. A., Giziewicz, J. B., Turner, L. A., and Smith, I. C. P., 1987, *Biochemistry*, **26,** 1805.
[119] Nallet, F., Roux, D., and Milner, S. T., 1990, *J. Phys., Paris*, **51,** 2333.
[120] Brink, D. M., and Satchler, G. R., 1968, *Angular Momentum*, 2nd edition (Clarendon Press).
[121] De Raedt, B., and Michel, K. H., 1979, *Phys. Rev.* B, **19,** 767.
[122] Pick, R. M., and Yvinec, M., 1980, *J. Phys., Paris*, **41,** 1053.
[123] Halle, B., 1992, *Liq. Crystals*, **12,** 625.
[124] Gustafsson, S., and Halle, B., *Molec. Phys.* (submitted).
[125] Freed, J. H., 1977, *J. chem. Phys.*, **66,** 4183.
[126] Galerne, Y., Figueiredo Neto, A. M., and Liébert, L., 1987, *J. chem. Phys.*, **87,** 1851.
[127] Fontell, K., Fox, K. K., and Hansson, E., 1985, *Molec. Crystals, liq. Crystals*, **1,** 9.
[128] Charvolin, J., and Sadoc, J. F., 1988, *J. Phys., Paris*, **49,** 521.
[129] Moro, G., and Nordio, P. L., 1983, *Chem. Phys. Lett.*, **96,** 192.
[130] Ferrarini, A., Moro, G., and Nordio, P. L., 1992, *The Molecular Dynamics of Liquid Crystals*, edited by G. R. Luckhurst (Kluwer Academic) (in the press).
[131] Szabo, A., 1984, *J. chem. Phys.*, **81,** 150.
[132] Vold, R. R., and Vold, R. L., 1988, *J. chem. Phys.*, **88,** 1443.
[133] Halle, B., 1991, *J. chem. Phys.*, **94,** 3150.
[134] Halle, B., Ljunggren, S., and Lidin, S., 1992, *J. chem. Phys.*, **97,** 1401.
[135] Zannoni, C., 1979, *The Molecular Physics of Liquid Crystals*, edited by G. R. Luckhurst and G. W. Gray (Academic Press), p. 51.
[136] Halle, B., 1984, *Molec. Phys.*, **53,** 1427.
[137] Halle, B., 1985, *Molec. Phys.*, **56,** 209.
[138] Halle, B., 1987, *Molec. Phys.*, **60,** 319.
[139] van Kampen, N. G., 1981, *Stochastic Processes in Physics and Chemistry* (North-Holland).
[140] Landau, L. D., and Lifshitz, E. M., 1986, *Theory of Elasticity*, 3rd edition (Pergamon Press).
[141] Leslie, F. M., 1966, *Quart. J. Mech. Appl. Math.*, **19,** 357.
[142] Brochard, F., 1973, *J. Phys., Paris*, **34,** 411.
[143] Blinc, R., Luzar, M., Vilfan, M., and Burgar, M., 1975, *J. chem. Phys.*, **63,** 3445.
[144] Freed, J. H., 1992, *J. chem. Phys.*, **96,** 3901.
[145] Vold, R. L., Vold, R. R., and Warner, M., 1988, *J. chem. Soc. Faraday Trans. 2*, **84,** 997.
[146] Vold, R. R., and Vold, R. L., 1988, *J. chem. Phys.*, **88,** 4655.
[147] de Gennes, P. G., 1969, *J. Phys. Colloque, Paris*, **C30,** 65.
[148] Nallet, F., Roux, D., and Prost, J., 1989, *J. Phys., Paris*, **50,** 3147.
[149] Selinger, J. V., and Bruinsma, R. F., 1991, *Phys. Rev. A*, **43,** 2910.
[150] Blinc, R., 1976, *NMR Basic Principles and Progress*, Vol. 13, edited by M. M. Pintar (Springer-Verlag), p. 97.
[151] Ukleja, P., Pirs, J., and Doane, J. W., 1976, *Phys. Rev.* A, **14,** 414.
[152] van der Zwan, G., and Plomp, L., 1989, *Liq. Crystals*, **4,** 133.
[153] Chan, D. Y. C., and Halle, B., 1984, *Biophys, J.*, **46,** 387.
[154] Goetz, A., 1970, *Introduction to Differential Geometry* (Addison-Wesley).
[155] Kékicheff, P., and Tiddy, G. J. T., 1989, *J. phys. Chem.*, **93,** 2520.
[156] Seddon, J. M., 1990, *Biochim. biophys. Acta*, **1031,** 1.
[157] Mariani, P., Luzzati, V., and Delacroix, H., 1988, *J. molec. Biol.*, **204,** 165.
[158] Scriven, L. E., 1976, *Nature, Lond.*, **263,** 123.
[159] Larsson, K., Fontell, K., and Krog, N., 1980, *Chem. Phys. Lipids*, **27,** 321.
[160] Longeley, W., and McIntosh, J., 1983, *Nature, Lond.*, **303,** 612.
[161] Hyde, S. T., Andersson, S., Ericsson, B., and Larsson, K., 1984, *Z. Kristallogr.*, **168,** 213.
[162] Charvolin, J., and Sadoc, J. F., 1987, *J. Phys., Paris*, **48,** 1559.
[163] Nitsche, J. C. C., 1989, *Lectures on Minimal Surfaces*, Vol. 1, (Cambridge University Press).
[164] Schoen, A., 1970, *N.A.S.A. Tech. Rep.*, D-5541.
[165] Bruinsma, R., 1992, *J. Phys., II, Paris*, **2,** 425.
[166] Szabo, A., 1980, *J. chem. Phys.*, **72,** 4620.
[167] Anderson, D., Wennerström, H., and Olsson, U., 1989, *J. phys. Chem.*, **93,** 4243.

[168] LIDIN, S., 1988, *J. Phys., Paris*, **49**, 421.
[169] CHARVOLIN, J., 1983, *J. Chim. phys.*, **80**, 15.
[170] HOFFMANN, H., 1984, *Ber. Bunsenges. phys. Chem.*, **88**, 1078.
[171] SAUPE, A., 1984, *Nuovo Cim.*, **3**, 16.
[172] BODEN, N., CORNE, S. A., HOLMES, M. C., JACKSON, P. H., PARKER, D., and JOLLEY, K. W., 1986, *J. Phys., Paris*, **47**, 2135.
[173] SONIN, A. S., 1987, *Sov. Phys. Usp.*, **30**, 875.
[174] GALERNE, Y., 1988, *Molec. crystals liq. Crystals*, **165**, 131.
[175] KUZMA, M. R., 1985, *J. phys. Chem.*, **89**, 4124.
[176] ZANNONI, C., 1992, *The Molecular Dynamics of Liquid Crystals*, edited by G. R. Luckhurst (Kluwer Academic) (in the press).
[177] AMARAL, L. Q., and HELENE, M. E. M., 1988, *J. phys. Chem.*, **92**, 6094.
[178] MAIER, W., and SAUPE, A., 1959, *Z. Naturf.* (*a*), **14**, 882.
[179] LUCKHURST, G. R., 1979, *The Molecular Physics of Liquid Crystals*, edited by G. R. Luckhurst and G. W. Gray (Academic Press), p. 85.
[180] VOLD, R. R., and VOLD, R. L., 1992, *The Molecular Dynamics of Liquid Crystals*, edited by G. R. Luckhurst (Kluwer Academic) (in the press).